DIRECT CONTACT HEAT TRANSFER BETWEEN IMMISCIBLE LIQUIDS

Samuel Sideman

Department of Chemical Engineering
Technion, Israel Institute of Technology, Haifa, Israel

I. Introduction

Direct heat and mass transfer between dispersed and continuous liquid phases is utilized over a wide range of industrial applications. The advantages of direct-contact heat transfer over the conventional processes using metallic transfer surfaces have lately stimulated research on its utilization for water

desalination projects. These advantages, predominant factors in determining the feasibility of the various suggested projects, are

(1) Simple design and relatively inexpensive equipment;
(2) Low maintenance due to absence, or reduction, of scale formation on solid surfaces;
(3) The obtainable close temperature approaches.

The larger volumes of fluids required in liquid–liquid heat transfer can sometimes be reduced by having the dispersed phase evaporate (or condense) within the continuous liquid medium. Latent, rather than sensible, heat transfer takes place in these "three-phase" exchangers, thus permitting a more effective heat-transfer process. Though this method is promising, relatively little is known about direct-contact heat transfer between immiscible liquids. The basic characteristics of heat transfer between dispersed and continuous media are thus of both scientific and practical interest.

Although most of the literature dealing with single drops is confined to mass transfer, the pertinent information is reported here in heat-transfer terms, using the classical analogies. However, interfacial agitation, regarded as concentration-dependent rather than temperature-dependent, may have affected some of the empirical equations in question. Hence care must be exercised when applying the latter to actual liquid–liquid heat-transfer operations.

The passage of a drop through a column of another liquid is characterized by three regimes: (*a*) drop formation and acceleration; (*b*) constant velocity; and (*c*) coalescense. In the present work the constant-velocity region is treated in detail in Sections II and III, whereas reference to the other two regions is made in Section VI. Section III deals with the fundamental case of a freely moving drop in a constant-temperature liquid. Section IV is mainly devoted to the interesting and highly important case of spray columns, where the drops move in a liquid under continuous temperature change. In Section V, the relatively new "three-phase" direct-contact heat transfer with change of phase is discussed. The various aspects of column end effects, drop temperature, and drop diameter are treated in Section VI.

The basic "classical" theories, such as the film, boundary layer, transient film, and penetration hypotheses are obviously outside the scope of this chapter, but the reader is assumed to be familiar with their basic concepts. Harriott's (H8) recent review on mass transfer to interfaces is recommended in this connection. An excellent treatise on the motion of drops and bubbles in fluid media is found in Levich's "Physicochemical Hydrodynamics" (L8, Ch. 8).

The two-film concept is convenient in describing transfer phenomena. However, use of this general concept, applicable even to agitated fluids near the interface, should not be taken as support for the classical stagnant film

hypothesis, better known as the "two-film theory." Instead, the general concepts of Toor's (T5) combined film penetration theory should preferably be borne in mind.

To adopt a common procedure here, the external film coefficient is expressed in terms of the Nusselt number. The internal coefficients, however, are given indirectly by the transfer efficiency, E_m, representing the fractional approach to the maximum possible heat transfer. Thus, by definition,

$$E_m \equiv \left(\frac{T_0 - T_i}{T_c - T_i}\right)$$

where T_0 and T_i are the outlet and inlet mixing-cup average temperatures of the drop, and T_c is the constant temperature of the continuous medium. With heat capacities assumed to be constants, E_m is the ratio of the heat actually absorbed by the drop to the maximum transferable heat. The internal heat-transfer coefficients (defined as the actual amount of heat transferred per unit area, time, and temperature gradient), can conveniently be expressed in terms of E_m and drop area. Plots are available for this conversion (B15). It should be noted that E_m as defined here is confined to the constant-velocity region and is only identical with the over-all transfer efficiency, E_T, provided end effects are disregarded.

Despite intensive efforts towards better understanding of transfer phenomena between drops and continuous media, accurate prediction of the transfer coefficients for a given system can as yet only be hoped for. Nevertheless, accumulated experience may provide an indication of the transfer mechanism to be encountered and the relevant coefficients may be estimated accordingly. Conversely, given experimental data, the controlling mechanism may be defined. It is therefore of theoretical as well as of practical interest to survey, in as much detail as space allows, the commonly postulated models and suggested mechanisms of transfer to single drops (S8). Since most of the analyses are reported in terms of dimensionless groups, attempts to obtain general equations by dimensional analysis, as well as their inherent limitations, will be dealt with first.

II. Equations Based on Dimensionless Similarity

Similarity criteria are ratios of the various forces or fluxes controlling the rate of the process involved. These are the momentum, viscous, gravity, and surface-tension forces and the conduction and convection terms, determined by the geometry of the system and the physical properties of the fluids. Density, viscosity, surface tension, heat capacity, and thermal conductivity are the physical properties to be considered.

The dimensionless equation describing the transfer phenomena may be obtained either by direct reference to the ratios of the physical quantities or by recourse to the classical techniques of dimensional analysis, i.e., the Buckingham Π Theorem or Rayleigh's method of indices. In addition, the basic differential equations governing the process may be reduced to dimensionless form and the coefficients identified. In general, the dimensionless equation for heat transfer through the combined film is

$$N_{Nu} = f\left(N_{Re}, N_{Pr}, N_{We}, \frac{\rho_d}{\rho_c}, \frac{\mu_d}{\mu_c}, \frac{\alpha_d}{\alpha_c}\right) \tag{1}$$

However, if each of the films is considered separately, two equations similar to Eq. (1), but excluding the diffusivity-ratio term, are obtained (H5). Determination of the functional relationship between the various dimensionless groups is quite difficult, and many of the correlations reported (see Tables I–III) are abbreviated forms of Eq. (1). Obviously these introduce the assumption that effects of interfacial tension, phase viscosities, and density difference on the transfer coefficient are constant over the usual range of these properties. Since the range is normally narrow, the assumption is quite reasonable, though one may expect a fairly wide scatter of measured values for unusual systems.

An attempt to combine in a single dimensionless equation the numerous variables involved in extraction from a drop was reported recently. Lileeva and Smirnov (L14) derived the dimensionless groups from the four basic differential equations (motion, continuity, kinetic diffusion, and convection) and the initial and boundary conditions. The eleven groups derived were then reduced to the following equation:

$$(N_{Nu})_c = 2.44 \times 10^{-12}(N_{Re})_d^{0.9}(N_{Re})_c^{0.2}(N_{Pr})_d^{0.5}(N_{Pr})_c^{0.5}(N_{Fo})^{-0.14}(N_{Gr})^{1.2}K^{-0.5}L^{-1.5} \tag{2}$$

where N_{Fo} is the Fourier number, N_{Gr} the Grashof number, K the log-mean average of the distribution coefficients, and L a geometrical factor relating the drop and column diameters.

A large number of independent experiments is required to determine the functional relationship between the various dimensionless groups. Moreover, some of the groups are interrelated. The exponents of the relationship proposed in Eq. (2) were determined by assigning values to the exponents of the standard groups (N_{Re}, N_{Pr}) and, by trial and error, the numerical values of the other exponents were adjusted to fit the experimental data. Thus, though this relationship is applicable to extraction of acids from benzene drops into water, it cannot, by nature of its derivation, be considered as general.

III. Heat Transfer to Drops Moving in a Constant-Temperature Field

A. Assumed Physical Models

A common, and more rigorous, procedure is based on deriving an equation from an assumed physical model, susceptible to mathematical analysis, and evaluating the assumptions of the model by means of experimental data. The three models to be discussed here are

(a) Rigid drop;
(b) Completely mixed drop;
(c) Drop with internal circulation.

As already stated, it is not uncommon to determine the transfer mechanism for a given system by comparing the experimental data with theoretical values calculated from the corresponding models (M3). A method for testing experimental data with a view to determining the applicable transfer mechanism was suggested by Licht and Pansing (L13). The method, based on plotting $\log(1 - E_T)$ vs time, is especially suitable for cases with long contact time. In the present chapter the mechanisms based on the above-mentioned models are studied with special emphasis on model (c). The various theoretical and empirical equations obtained by means of these models are summarized in Tables I–IV.

B. Rigid-Drop Model

This model is obviously an extension of the well-known theory of heat transferred by radial conduction. Solution of the basic differential equations depends on the boundary conditions stipulated, the boundary layer and velocity profiles of the continuous phase.

1. *Transfer Coefficients outside a Rigid Drop*

Numerous workers (B16, F2, F4, H17, J4, K4, K7, L8, M2, S5, and others) estimated the external heat-transfer coefficient in the continuous phase by assuming a velocity profile in the boundary layer and ambient fluid. Except for very low Reynolds numbers, the exact boundary layer solutions only apply to the front part of the drop, up to the separation point. Fortunately, simple assumptions sometimes suffice for extending the derivation to the entire drop, and the relationships obtained are in agreement with experimental data. The limitations of the analytical solutions, as well as their application to nonspherical drops, is concisely demonstrated in Lochiel and Calderbank's (L18) recent study on mass transfer around axisymmetric bodies of revolutions.

TABLE I

EQUATIONS FOR OUTSIDE NUSSELT NUMBER $[(N_{Re})_c < 1]$: RIGID-DROP MODEL

Equation no.	Source	$(N_{Nu})_c$	$(N_{Re})_c$	$(N_{Pr})_c$	$(N_{Pe})_c$	Physical description	Derivation
I-1	(F2)	$2 + \frac{(N_{Pe})_c}{2} + \frac{(N_{Pe})_c^2}{6} + \cdots$	<1	—	<1	Laminar flow Thick concentration boundary layer	Boundary layer theory Stokes stream function
I-2	(W3)	$2 + \frac{9}{16}(N_{Pe})_c + \frac{9}{64}(N_{Pe})_c^2 + \cdots$	<1	—	<1	Laminar flow Thick concentration boundary layer	Boundary layer theory approximated from (B12)
I-3	(F3)	$2 + 0.32(N_{Pe})_c^2$	<1	—	<1	Laminar flow	Perturbation method
I-4	(K6)	$2 + 0.5(N_{Pe})_c + 0.3(N_{Pe})_c^2$	<1	—	<1	Laminar flow	Perturbation method
I-5	(B14)	$2 + \frac{1}{2}(N_{Pe})_c + \frac{1}{4}(N_{Pe})_c^2 \ln(N_{Pe})_c + \cdots$	<1	—	<10	Laminar flow	Perturbation method
I-6	(F2)	$0.89(N_{Pe})_c^{1/3}$	<1	—	$>10^3$	Laminar flow Thin concentration boundary layer	Boundary layer theory Stokes stream function
I-7	(B12, F2, W3)	$0.98(N_{Pe})_c^{1/3}$	<1	—	$>10^3$	Laminar flow Thin concentration boundary layer	Boundary layer theory Stokes stream function
I-8	(A1)	$1.075(N_{Pe})_c^{1/3}$	<1	$\gg 1$	—	Liquid–solid mass transfer	Boundary layer theory and empiricism

In general, correlations for $N_{Pe} < 1$, $N_{Re} < 1$ have the following form:

$$(N_{Nu})_c = \text{Polynomial}(N_{Pe}) \tag{3}$$

where $N_{Pe} = N_{Re} \cdot N_{Pr}$. Some of these relations are presented in Table I and compared in Fig. 1.

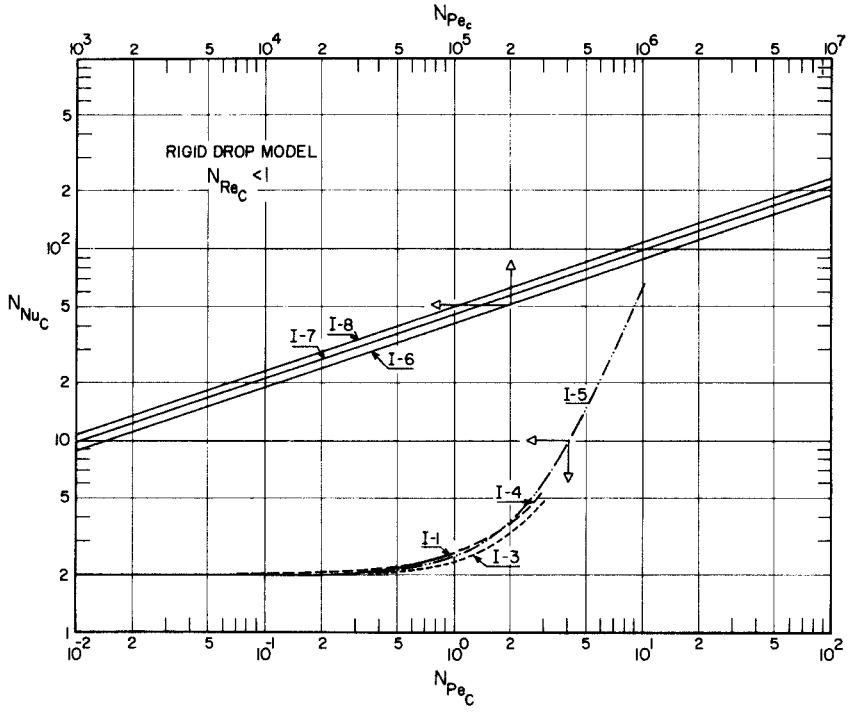

FIG. 1. Comparison of equations for outside Nusselt number (cf. Table I).

For the more common and practical operating range of $N_{Pe} > 1$, Eq. (1) reduces to

$$(N_{Nu})_c = a + b(N_{Re})_c^m (N_{Pr})_c^n \tag{4}$$

where

$$m = n = \tfrac{1}{3} \quad \text{for} \quad N_{Pe} \gg 1; \quad N_{Re} < 1$$

and

$$m = \tfrac{1}{2} \qquad n = \tfrac{1}{3} \qquad \text{for} \quad 1 < (N_{Re})_c < 10^4$$

The constants a, b, m, and n, as determined by various workers in the field, are seen in Table II. Some of the proposed equations for $(N_{Re})_c > 1$ are

TABLE II

EQUATIONS FOR OUTSIDE NUSSELT NUMBER $[(N_{Re})_c > 1]$: RIGID-DROP MODEL

Equation no.	Source	$(N_{Nu})_c$	$(N_{Re})_c$	$(N_{Pr})_c$	Physical description	Derivation
II-1	(A1)	$0.8\,(N_{Re})_c^{1/2}\,(N_{Pr})_c^{1/3}$	$1 \ll - < 10^4$	>1	Dissolving of solids	Boundary layer theory and empiricism
II-2	(F4, G12)	$2 + 0.55\,(N_{Re})_c^{1/2}\,(N_{Pr})_c^{1/3}$	2–1000	<1	Evaporation and sublimation	Empirical
			20–160	>1	Mass transfer, liquid–liquid	Empirical
II-3	(R3, R2)	$2 + 0.60\,(N_{Re})_c^{1/2}\,(N_{Pr})_c^{1/3}$	0–200 $1\text{–}7 \times 10^4$	<1	Evaporation	Empirical
II-4	(H18)	$2 + 0.54\,(N_{Re})_c^{1/2}\,(N_{Pr})_c^{1/3}$	50–350	1–2	Evaporation	Empirical
II-5	(T1, G21)	$2.1 + 0.42\,(N_{Re})_c^{1/2}\,(N_{Pr})_c^{1/3}$	50–1000	1	Evaporation	Empirical
II-6	(R1)	$2.83 + 0.60\,(N_{Re})_c^{1/2}\,(N_{Pr})_c^{1/3}$	50–1000	1	Evaporation	Empirical
II-7	(G21)	$2 + 0.57\,(N_{Re})_c^{1/2}\,(N_{Pr})_c^{0.35}$	>1	>1	Mass transfer, gas–liquid	Empirical
II-8	(K2)	$2 + 0.57f(N_{Re})_c^{1/2}\,(N_{Pr})_c^{1/2}$	0–2500	1	Mass transfer	Empirical
II-9	(G11)	$2 + 0.95\,(N_{Re})_c^{1/2}\,(N_{Pr})_c^{1/3}$	60–600	>1	Mass transfer, liquid–solid	Empirical
II-10	(G4)	$44 + 0.48\,(N_{Re})_c^{1/2}\,(N_{Pr})_c^{1/3}$	20–835	>1	Mass transfer, liquid–solid	Empirical
II-11	(W11, G4)	$1.45\,(N_{Re})_c^{0.35}\,(N_{Pr})_c^{1/3}$	4–400	$\gtrsim 1$	Mass transfer, evaporation	Empirical
II-12	(W11, L16)	$0.43\,(N_{Re})_c^{0.56}\,(N_{Pr})_c^{1/3}$	400–10^5	1	Mass transfer, gas–liquid solid–liquid	Empirical
II-13	(K4)	$2 + 1.3\,(N_{Pr})_c^{0.15} + 0.66\,(N_{Re})_c^{1/2}\,(N_{Pr})_c^{0.31}$	0.4–10^5	0.7–400	Heat transfer	Empirical
II-14	(V2)	$[1.2 + 0.53\,(N_{Re})_c^{0.54}]\,(N_{Pr})^{0.3}\left(\frac{\mu_c}{\mu_d}\right)^{0.25}$	$1\text{–}3 \times 10^5$	2–380	Heat transfer	Empirical
II-15	(M2, C1)	$[0.97 + 0.68\,(N_{Re})_c^{1/2}]\,(N_{Pr})_c^{0.3}$	$<10^3$	<400	Heat transfer	Empirical
II-16	(S20)	$(N_{Nu})_0 + 0.347\,(N_{Re})_c^{0.62}\,(N_{Pr})_c^{0.31}$ [b]	$<10^4$	0.7–380	Heat transfer	Empirical

[a] f rises to about 2 as $(N_{Re})_c$ goes from 0 to 10, then falls slowly to 1; $f = 1$ for $(N_{Re})_c > 80$.

[b] $(N_{Nu})_0 = 2 + 0.569\,[(N_{Gr})_c(N_{Pr})_c]^{0.25}$.

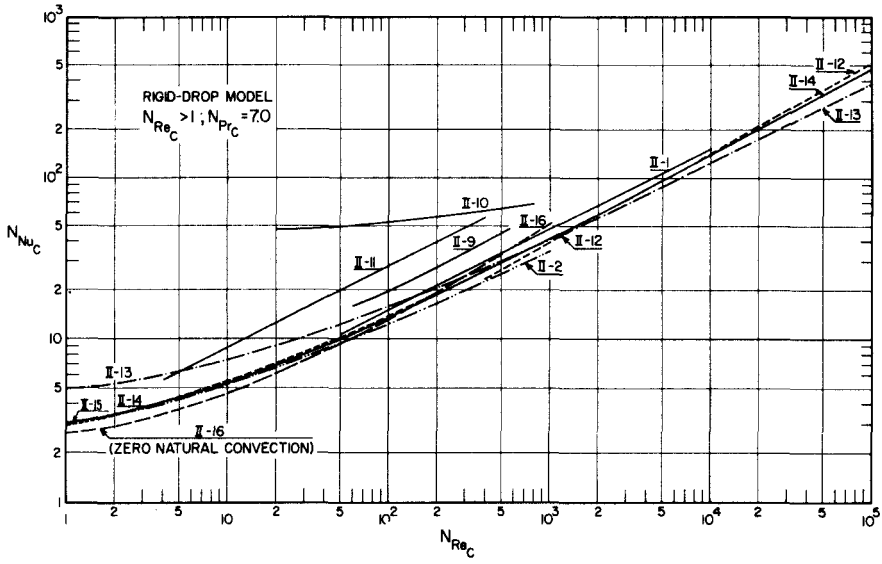

FIG. 2. Comparison of equations for outside Nusselt number (Table II).

compared in Fig. 2. The continuous phase was taken as water, with $(N_{Pr})_c = 7$. Some other references, dealing with boundary layer solutions for solid spheres and not included here, are given in (G21, H17, S20). As seen from Table II, most transfer data for solid spheres and stagnant drops up to Reynolds numbers of 1000 fit Eq. (4), with b varying between 0.43 and 0.95, the higher value most probably suitable for liquid–liquid systems. In general, $b = 0.57$ is recommended (G21) and

$$(N_{Nu})_c = 2 + 0.57(N_{Re})_c^{1/2}(N_{Pr})_c^{1/3} \tag{5}$$

$(N_{Nu})_c = a = 2$ is the limiting value for diffusion into infinite stagnant medium, originally calculated by Langmuir (L3) in 1918 and confirmed since by numerous workers. However, as natural convection may be pronounced in liquid systems, higher limiting values may be obtained, especially with large spherical drops moving in liquids with low kinematic viscosities ν, since for natural convection the Grashof number varies inversely as ν^2 and directly as cube of the diameter. Good agreement was obtained with $b = 0.95$ for liquid–liquid and liquid–solid systems. However, a more general equation, suggested by Steinberger and Treybal (S20), based on the additivity of natural and forced convection and valid for all systems (including gas–liquid), is shown in Fig. 3:

$$(N_{Nu})_c = (N_{Nu})_0 + 0.347(N_{Re})_c^{0.62}(N_{Pr})_c^{0.31} \tag{6}$$

TABLE III EQUATIONS FOR OUTSIDE

Equation no.	Source	$(N_{Nu})_c$	$(N_{Re})_c$
III-1	(L8)	$0.65(N_{Pe})_c^{1/2}\left(\frac{\mu_c}{\mu_c+\mu_d}\right)^{1/2}$	<1
III-2	(G21)	$0.67(N_{Pe})_c^{1/2}\left(\frac{\mu_c}{\mu_d+\mu_c}\right)^{1/2}$	<1
III-3	(W3)	$0.61(N_{Pe})_c^{1/2}\left(\frac{\mu_c}{\mu_d+\mu_c}\right)^{1/2}$	<10
III-4	(G21)	$0.89(N_{Pe})_c^{1/3}\left(\frac{\mu_d+1.33\mu_c}{\mu_d+\mu_c}\right)^{1/3}$	<1
III-5	(W3)	$0.98(N_{Pe})_c^{1/3}\left(\frac{\mu_d+1.58\mu_c}{\mu_d+\mu_c}\right)^{1/3}$	<10
III-6	(W3)	$2+\frac{9}{16}(N_{Pe})_c+\frac{9}{64}(N_{Pe})_c^2+\cdots$	<10
III-7	(B14)	$2+\frac{1}{2}(N_{Pe})_c+\frac{1}{4}\left(\frac{2\mu_c+3\mu_d}{3\mu_c+3\mu_d}\right)(N_{Pe})_c^2\ln(N_{Pe})_c+\cdots$	<1
III-8	(B6)	$1.25(N_{Pe})_c^{1/2}$	—
III-9	(B10)	$1.13(N_{Pe})_c^{1/2}$	—
III-10	(G21)	$2+1.13(N_{Pe})_c^{1/2}K_v^{1/2}$	>1
III-11	(G21) (C5)	$(N_{Nu})_{rigid}(1-K_v)^{-1/2}$	>1
III-12	(E2)	$\left(\frac{12}{\pi}\right)^{1/2}(N_{Pe})_c^{1/2}$	>1
III-13	(H13)	$g(N_{Pe})_c^{1/2}$	>1
III-14	(G12)	$0.6(N_{Pe})_c^{1/2}$	>1
III-15	(E2)	$5.52\left(\frac{\mu_c+\mu_d}{2\mu_c+3\mu_d}\right)^{3.47}\left(\frac{D\sigma\rho_c}{\mu_c^2}\right)(N_{Pe})_c^{1/2}$	<1500
III-16	(G3)	$-126+1.8(N_{Re})_c^{1/2}(N_{Pr})_c^{0.42}$	18–800
III-17	(T3)	$-178+3.62(N_{Re})_c^{1/2}(N_{Pr})_c^{1/3}$	50–800
III-18	(G12)	$50+8.5\times10^{-3}(N_{Re})_c(N_{Pr})_c^{0.7}$	100–700

$(N_{Pr})_c$	$(N_{Pe})_c$	Physical description	Derivation
—	$\gg 1$	Drop circulation	Hadamard steam function
—	$\gg 2.4\left(3\frac{\mu_d}{\mu_c}+4\right)^2\left(\frac{\mu_d}{\mu_c}+1\right) \gg 1$	Drop circulation	"Potential theory" plus Hadamard's velocity
—	$\gg 2.8\left(\frac{\mu_d+\mu_c}{\mu_c}\right)\left(\frac{12\mu_d+19\mu_c}{\mu_c}\right)^2$ $\gg 1$	Drop circulation	Hadamard stream function, approximation from (B12)
—	$\ll 2.4\left(3\frac{\mu_d}{\mu_c}+4\right)^2\left(\frac{\mu_d}{\mu_c}+1\right)$	Drop circulation	Hadamard stream function
—	$\ll 2.8\left(\frac{\mu_d+\mu_c}{\mu_c}\right)\left(\frac{12\mu_d+19\mu_c}{\mu_c}\right)^2$ >1000	Drop circulation	Hadamard stream function, approximation from (B12)
—	<1	Drop circulation	Hadamard stream function, approximation from (B12)
—	<10	Drop circulation	Perturbation technique
—	2–100	Drop circulation	Potential flow
—	Large	Drop circulation	Potential flow
>1	—	Drop circulation	Potential, modified
>1	—	Drop circulation	Reynolds analogy
—	Large	Drop circulation	Simplified boundary-layer theory
>1	—	Drop circulation	Empirical, mass transfer: gas–liquid; liquid–liquid
>1	—	Drop circulation	Empirical, mass transfer: liquid–liquid
>1	—	Drop circulation	Empirical, heat transfer: liquid–liquid
$\gg 1$	—	Drop circulation	Empirical, mass transfer: liquid–liquid
$\gg 1$	—	With and without circulation	Empirical, mass transfer: liquid–liquid
>1	—	Drop circulation plus oscillation	Empirical, mass transfer: liquid–liquid

TABLE IV INSIDE TRANSFER-EFFICIENCY EQUATIONS: RIGID- AND CIRCULATING-DROP MODELS (S8)

Eq. no.	Source	E_m	Eigenvalue	Description	Derivation
IV-1	(N3)	$1-\frac{6}{\pi^2}\sum_{n=1}^{\infty}\frac{1}{n^2}\exp\left[\frac{-\pi^2 n^2\alpha\theta}{R^2}\right]$		Rigid sphere: $h_c=\infty$, $T_c=$ const	Conduction equation
IV-2	(V1)	$\left[1-\exp\left(\frac{-\pi^2\alpha\theta}{R^2}\right)\right]^{1/2}$		Rigid sphere: $h_c=\infty$, $T_c=$ const	Empirical, Eq. (IV-1)
IV-3	(G22)	$1-6\sum_{n=1}^{\infty}A_n\exp\left[\frac{-\lambda_n^2\alpha\theta}{R^2}\right]$	Table A-1	Rigid sphere: $h_c\neq\infty$, $T_c=$ const	Conduction equation
IV-4	(K5)	$1-\frac{3}{8}\sum_{n=1}^{\infty}A_n^2\exp\left[\frac{-\lambda_n 16\alpha\theta}{R^2}\right]$	Table A-2	Drop circulation: $h_c=\infty$, $T_c=$ const, $\sigma=0$, $N_{Re}<1$	Hadamard stream function
IV-5	(E2)	$1-\frac{3}{8}\sum_{n=1}^{\infty}A_n^2\exp\left[\frac{-\lambda_n 16\alpha\theta}{R^2}\right]$	Table A-3	Drop circulation: $h_c\neq\infty$, $T_c=$ const, $\sigma=0$, $N_{Re}<1$	Hadamard stream function
IV-6	(C1)	$\left[1-\exp\left(\frac{-2.25\pi^2\alpha\theta}{R^2}\right)\right]^{1/2}$		Drop circulation: $h_c=\infty$, $T_c=$ const, $10<N_{Re}<200$, $6<N_{Pr}<3000$	Empirical, Eq. (IV-4)
IV-7	(H5)	$1-2\sum_{n=1}^{\infty}A_n^2\exp\left[\frac{-\lambda_n\alpha\theta(N_{Pe'})_d}{512R^2}\right]$	$\lambda_1=2.88$	Drop circulation allowed with a radial motion: $N_{Re}=1000$, $h_c=\infty$, $T_c=$ const	Einstein equation
IV-8	(J2)	$1-6\sum_{n=1}^{\infty}A_n\exp\left[\frac{-\lambda_n^2\bar{R}\alpha\theta}{R^2}\right]$	Table A-1	Drop circulation or oscillation: $10<N_{Re}<120$, $315<N_{Re}<620$	Empirical, Eq. (IV-3)
IV-9	(J2)	$0.905\left(\frac{\bar{R}\pi^2\alpha\theta}{R^2}\right)^{1/2}+0.0189$		Drop circulation or oscillation: $E_m<0.5$	Curve fitting, Eq. (IV-8)
IV-10	(J2)	$1-6A_1\exp[-\lambda_1^2\bar{R}\alpha\theta/R^2]$	Table A-1	Drop circulation or oscillation: $E_m>0.5$	Eq. (IV-8)

where

$$(N_{Nu})_0 = 2 + 0.569[(N_{Gr})_c(N_{Pr})_c]^{0.25} \tag{7}$$

is the natural-convection contribution to transfer, when $(N_{Gr})_c \cdot (N_{Pr})_c < 10^8$.

Oscillation of the wake, already setting in at Reynolds numbers of about 200 for stagnant drops and 500 for solid spheres (G12), as well as of the drops, increases the transfer rate. Direct proportionality between the transfer coefficient and $(N_{Re})_c$ may be approached (G12). This is probably why Steinberger and Treybal (S20) found that the exponent $m = 0.62$ for Reynolds

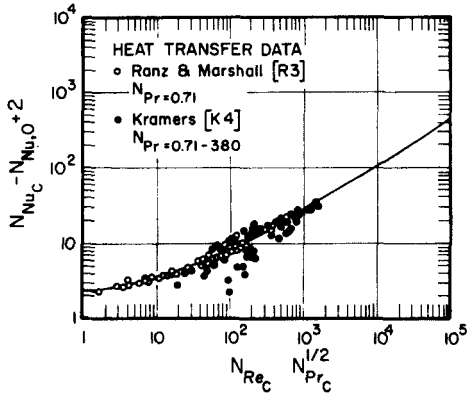

FIG. 3. Comparison of Eq. (6) with literature data (S20). (Courtesy of American Institute of Chemical Engineers.)

number gave the best fit in their general correlation, in the extended range of $1 < (N_{Re})_c < 30000$. If transfer in the wake region is assumed to obey the transient film mechanism postulated by the penetration theories of Higbie (H15) or Danckwerts (D2), an exponent higher than $n = \frac{1}{3}$ would be expected for the Prandtl number. However, Eqs. (5) or (6) should be satisfactory for most dispersed-phase problems, where fluid spheres would not exceed $(N_{Re})_c = 1000$.

It is of interest to note that, by judicious definition of the characteristic diameter of nonspherical bodies, good agreement with the equations for spherical solids was obtained. A diameter defined by the total surface area of the body, divided by the perimeter normal to flow, was successfully used for spheres, hemispheres, cubes, prisms, and cylinders (P1), yielding $a = 0$; $b = 0.692$; $m = 0.514$; and $n = \frac{1}{3}$ [Eq. (4)]. Similar results were obtained for spheroids (S14), namely $a = 0$; $b = 0.74$; $m = 0.5$; and $n = \frac{1}{3}$. The commonly used equivalent diameter of a sphere of the same volume as the body yields transfer coefficients increasing with eccentricity (S14).

2. *Transfer Coefficients inside a Rigid Drop*

Newman (N3), Geddes (G16), and others obtained the internal transfer efficiency, for the special case of zero resistance of the external film. By solving the unsteady-state diffusion equation, they obtained the following expression for the transfer efficiency:

$$E_m = 1 - \frac{6}{\pi^2} \sum_{n=1}^{\infty} \frac{1}{n^2} \exp\left[- \frac{\pi^2 n^2 \alpha_d \Theta}{R^2} \right] \tag{8}$$

where α is the thermal diffusivity, Θ the time, and R the radius of the drop.

Evidently Eq. (8) yields the highest transfer coefficient for small drops (less than 1–2 mm. diam.), mainly encountered in agitating systems where the rigid-drop model should apply.

The transfer efficiency, calculated by Brown (B15) as a function of time for various water-drop diameters, is presented in Fig. 4, indicating the minimum residence time required for a given transfer efficiency.

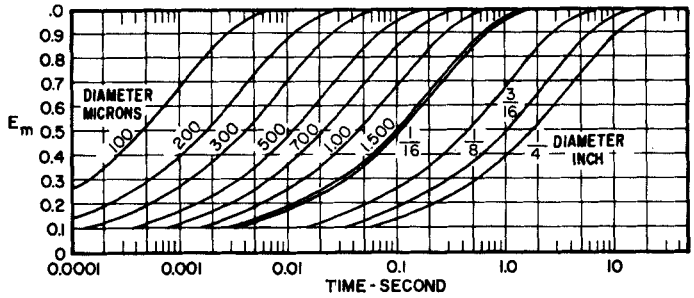

FIG. 4. Time of heating, by conduction, a sphere of water: Eq. (8), zero initial temperature, thermal diffusivity 0.0065 ft²/hr (B15). (Courtesy of American Society of Mechanical Engineers.)

A simplified solution based on experimental data was suggested by Vermeulen (V1):

$$E_m = \left[1 - \exp\left(- \frac{\pi^2 \alpha_d \Theta}{R^2} \right) \right]^{1/2} \tag{9}$$

An approximate solution applicable for $\alpha\Theta/R^2 < 10^{-2}$ can be obtained (H13) by using the solution for diffusion from a plane surface into an infinitely thick layer, which gives

$$E_m \simeq \frac{6}{\pi^{1/2}} \left(\frac{\alpha_d \Theta}{R^2} \right)^{1/2} \tag{10}$$

However, comparison of Eqs. (8), (9), and (10) (Fig. 10) shows Eq. (10) to yield somewhat higher values of E_m even in the limited range indicated here.

Grober (G22) and Jakob (J1) included the external film resistance, and obtained

$$E_m = 1 - 6\sum_{n=1}^{\infty} A_n \exp\left[-\frac{\lambda_n^2 \alpha \Theta}{R^2}\right] \tag{11}$$

A graphical solution of Eq. (11) is given by McAdams (M2). A modified form of this graph, suggested by Calderbank (C1), is presented in Fig. 5. The constants A_n and eigenvalues λ_n are given in the Appendix, Table A-I.

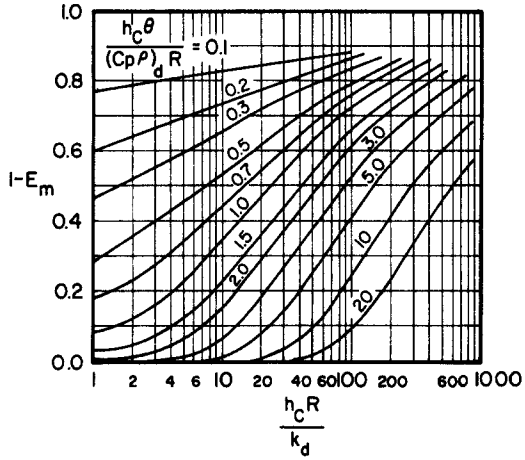

FIG. 5. Transfer efficiency by diffusion into spheres with finite continuous-phase resistance (C1). (Courtesy of *Chemical Engineering Science*.)

C. COMPLETELY MIXED-DROP MODEL

In accordance with the two-film theory, the two phases are considered to have uniform, though different, bulk temperatures. The over-all heat-transfer coefficient through the combined films U is defined by

$$dQ/d\Theta = AU(T_c - T_d) \tag{12}$$

where $dQ = (VC_p\rho T)_d$ is the heat transferred to the drop, and A and V are the surface area and volume of the drop, respectively. Integration over the duration of contact between the phases yields

$$E_m = 1 - \exp\left[-\left(\frac{A}{V\rho C_p}\right)_d U\Theta\right] \tag{13}$$

For the classical case of a completely mixed drop, where the internal film resistance is negligible compared with that of the external film, we have $U = h_c$; i.e., the external resistance governs the transfer rate.

Similarly, adaptation of the Higbie penetration theory for a completely mixed drop, with the contact time assumed to be identical with that required for the drop to traverse a distance equal to its diameter, yields [see also Eq. (29)]

$$E_m \simeq 1 - \exp\left[-3.39\left(\frac{\alpha_c \Theta}{R^2}\right)^{0.5}\right] \tag{14}$$

D. Drops with Internal Circulation

1. *General Characteristics of the Model*

Drop circulation is by far the most important and stimulating model and numerous workers have treated its momentum-, heat-, and mass-transfer aspects both theoretically[1] and experimentally.[2]

A drop (or bubble) moving in a viscous fluid tends to circulate internally (Fig. 6) due to the shear stress applied at its interface by the ambient fluid.

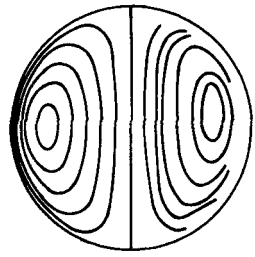

Fig. 6. Comparison of theoretical and experimental circulation patterns: glycerine drop in castor oil (S18).

As a result of the motion of the interface, the viscous friction is lower and the drop velocity higher. Hence the transfer rate is increased by a factor approximately equal to $1.9(N_{Pr})^{1/6}$ compared with the rigid drop. One may expect circulation to increase with drop size and the viscosity ratio μ_c/μ_d of the two fluids.

According to the classical theories of Hadamard (H2), Rybczynski (R9), and Boussinesq (B10), circulation sets in whenever a drop moves in a viscous fluid. Figure 6 shows Hadamard streamlines compared with the experimental ones obtained by Spelles (S18). Experiments (G8) indicated that circulation takes place readily, though not exclusively (G5), in the presence of a suitable driving force (temperature or concentration gradients) and only above a

[1] B4, B10, B12, D6, D7, F5, H2, H5, H15, K5, K6, L6, L7, L8, R8, R9, S3, and others.

[2] B13, C1, D8, E2, G3, G5, G6, G8, G12, G20, H4, H5, L15, L17, M3, R6, R8, S8, S18, T3, T4, and others.

certain level of the Reynolds number; i.e., whenever the drag force exceeds a certain minimum discussed below. The Reynolds number at which circulation sets in within the drop decreases with increasing viscosity of the continuous phase (G10).

Garner and Skelland (G9) suggested an equation for the critical Reynolds number determining the onset of circulation, but it is rather inaccurate since circulation is highly dependent on fluid purity and on the presence of surface active impurities (G5, G21, L17). The lower the interfacial tension, the lower the transitional Reynolds number (G8), and the higher the over-all transfer coefficient (L11, S6). For a drop with high surface tension, minute amounts of impurities suffice to produce an appreciable surface-tension gradient at the interface, thus greatly retarding circulation. Bond (B8, B9) included surface tension in his criterion for the onset of circulation, inferring that the latter was restricted by the interfacial tension when the radius was small enough. However, this criterion was derived from experimental data in the streamline region and is rather inadequate in the practical ranges of the Reynolds numbers, especially since circulation is known to be strongly affected by immeasurably small changes in surface tension due to surface active agents (D6, L17). Thus retardation of circulation is associated with surface-tension gradients along the interface, rather than a simple reduction in surface tension. For a given system, the effect of a surface-tension gradient increases with decreasing drop diameter, and below a certain size (as shown later) circulation is reduced or arrested with the transfer coefficients approaching the "rigid-drop" values.

It is now generally agreed that an adsorbed film of a surface active agent, which sets up tangential forces on the surface of the drop, is responsible for reducing or arresting drop circulation. The motion of the drop's interface causes a concentration gradient of the surface active agent, resulting in a gradient in the interfacial tension. [Polar oils are less susceptible, having lower energies of adsorption and higher rates of desorption of surface active material compared with nonpolar oils (D6).] The ensuing tangential forces are codirectional with the decreasing interfacial tension; they affect the flow characteristics at the interface by counterbalancing part of the shearing stress exerted by the continuous phase on the drop surface, and thereby reduce circulation. For a given system the resistance to circulation in the drop depends on its diameter; the smaller the drop, the larger will be the surface pressure gradient between its front and rear, and the smaller will be the tangential friction stress (D6). A force equilibrium at any point on the interface (G21, S4) gives

$$\frac{\partial \sigma}{\partial x} = \mu_c \frac{du_c}{dy} - \mu_d \frac{du_d}{dy} \tag{15}$$

where the x and y directions, respectively, are parallel and normal to the drop interface. Thus circulation within the drop will be retarded appreciably, or even arrested, if the interfacial tension gradient and external viscous drag are of the same order of magnitude. If the rear of the drop is covered beyond $\phi > 135°$, drag coefficients will correspond to the experimental values for solid spheres.

According to Savic (S3), Levich (L8), and others (D6, H3, L17), an immobile "cap" may be formed at the bottom of the drop, confining circulation to its front part only. This is due to the relatively small velocities at the vicinity of the rear stagnation point, and to accumulation of the surface active material near the point of flow separation (H3), if present. The resulting interfacial-tension gradient should prevent transmission of tangential stress to the interior fluid, thus creating a stagnant region in the rear part of the drop. This may explain why the second vortex ring inside the drop, predicted by Hamielec and Johnson (H3) for the intermediate range of Reynolds numbers, has never been observed.

If the rate of desorption of surfactants is very much greater than the rate at which the drop traverses through a distance equivalent to its diameter (about 0.02 sec), one may expect (D6) no accumulation of surfactants at the rear end. A quantitative semiempirical expression for the degree of drop circulation as a function of the viscous forces, drop diameter, densities and the compressional modulus of the surface film (surface-tension gradient), as well as the empirical fraction of liquid circulating, has been suggested by Davies (D6).

Levich (L8) and others (S4) have suggested a criterion for the critical drop diameter, incorporating the difference between the limiting interfacial tension σ_s (determined for large concentrations of surface active impurities) and that of the pure system σ. The proposed critical transition radius is given by Eq. 58 (Section VI,C). The dependence of circulation on the difference in interfacial tension has been experimentally verified (D6, G21), but no proof of the validity of this criterion has been reported. However, application of this criterion should provide approximate values.

It is of interest that the onset of circulation of liquid drops is associated with deformation of the spherical drop into an ellipsoid (R8, C6, G2). Deformation of the spherical drops was found to be associated with oscillations and with higher transfer rates (C6) even in highly viscous fluids where stagnant drop characteristics are generally assumed. Garner (G12), who studied the wake behind the deformed drops, concluded that the higher transfer rates were due to the onset of instability and oscillation of the wake at this relatively low Reynolds number (200) compared with 400 to 450 for solid spheres. However, no quantitative relationship is available.

Terjesen *et al.* (T3, B13) suggested that internal circulation in itself does

not account for the higher transfer coefficients of drops, compared with solid spheres. For pure fluids the higher transfer coefficients were accounted for by the higher velocities of circulating drops, rather than by the effect of circulation on the thickness of the external boundary layer. Drop velocity was found to be much more sensitive to the presence of surfactant than the transfer coefficients. "Solid-drop" velocities were reached at concentrations of surface active agent about 10 times lower than those required for the limiting reduction in the rate of mass transfer. Thus, if reduction in velocity represents reduction and eventual elimination of the internal circulation, they suggest that the higher mass-transfer rates realized are due to hydrodynamic causes such as formation of a vortex ring, rather than to internal circulation. This explanation is only partial, since the higher transfer rates measured with the noncirculating "slow" drops at low concentrations of the surfactants are related both to the area covered by the surfactant at the rear and to the turbulent wake characteristics.

The effect of the wake behavior and boundary layer separation on the rate of mass transfer was studied by Garner and Tayeban (G12). The volumes of the wakes behind highly viscous drops of about 300 cP viscosity, assumed stagnant, were found to be about twice those behind circulating drops of 6.5 cP viscosity. This corresponds to a large difference in the angle of boundary layer separation. Conkie and Savic (C5) suggest that the angle of separation for circulating spherical drops should be 108° (the same as for a solid sphere at higher Reynolds numbers). Garner showed that, for Reynolds numbers of 500, the angle for stagnant drops and for solid spheres is about 105°, whereas for circulating drops the value is 140°. Boundary layer separation was first observed at $(N_{Re})_c = 60$ for circulating drops of water in benzyl alcohol, compared with about 20 for solid spheres and stagnant drops. For fully circulating drops, the separation point should shift to the rear stagnation point, and no boundary layer separation should occur. The transfer coefficients should then approach the values predicted by potential-flow theory; Levich (F5, L8) reports that at $(N_{Re})_c = 300$ the turbulent wake of an uncontaminated gas occupies only an angle of 2° at the rear.

Thus, even for drops of low viscosity if not completely circulating, the interfacial velocity gradient is smaller and the contact area larger, resulting with higher transfer coefficients compared with stagnant "solid" spheres. For small drops, below 0.25 cm, the wake is nearly saturated, and steady transfer coefficients are obtained. The concentration in the wake decreases below the saturation value with increasing drop diameter and velocity, corresponding to higher Reynolds numbers and higher turbulence in the wake. Even with highly viscous drops, the onset of instability of the wake at $(N_{Re})_c = 160$ resulted in transfer coefficients higher by some 30% (G12). Thus the toroidal vortex, setting in under boundary layer separation at

Reynolds numbers of about 20 (in stagnant drops), gains strength as the separation point shifts at higher Reynolds numbers. The increase in transfer coefficient in the continuous phase, even for drops not fully circulating, may thus be attributed to the combined effect of the increased disturbance intensity around the separation point and in the wake, to the forward movement of the separation point, and to higher velocities.

The relative importance of the rear part of the drops compared with solid spheres was noted by Garner and also by Terjesen (T3). Garner (G4, G11) and others (A1) showed that at moderate Reynolds numbers, up to 2500, most of the transfer takes place in the front part of the solid spheres ahead of the separation point. However, no frontal diffusion into liquid drops could be detected at high rates of fall (G2), whereas it was readily noticeable behind the drop. Thorsen and Terjesen (T3) concluded that the relative importance of the front and rear for drops and solid spheres is reversed, beginning with Reynolds numbers above 20. This hypothesis does not account for the extreme case where internal circulation is reversed (L17), probably due to higher transfer rates at the front and to the nonnegligible internal resistance to transfer.

Another aspect, usually overlooked, is the effect of natural convection inside the drop on the transfer coefficient. Transfer coefficients differing by about 25% were found (W12) when drops were heated or cooled in the continuous phase (see Section IV,B).

A decrease of the transfer coefficient of drops and bubbles with time, due to decay of circulation, has been noted in a number of studies. Deindoerfer and Humphrey (D8) showed that the transfer coefficients of one- to two-second-old oxygen bubbles rising in water were in agreement with those obtained from the Higbie (H15) penetration theory, whereas the coefficients of six-second-old bubbles were close to those predicted by the rigid-drop theories. High absorption rates during the first few seconds after drop formation were also measured (G7) for single liquid drops suspended in a gas stream. Garner and Lane (G7) attributed such high rates to a high initial rate of circulation within the drop due to oscillations arising in the breaking away of the drop from the forming nozzle. They found a direct relation between circulation (as based on the flow adjacent to the interface) and the internal resistance to mass transfer, but none between drop oscillation and mass transfer inside the drop. However, recent cinecamera studies of Marsh and Heideger (M1a) on mass transfer to falling drops showed no oscillations of the newly formed drops upon separation from the forming nozzle. The very high mass-transfer rates in the first second following formation were attributed to the presence of disordered internal motion caused by the high velocity of the liquid comprising the drop. An approximate mathematical

model predicting the decay of the transfer coefficient was applied with apparent success (M1a). The sharp decrease in the transfer coefficient may thus be understood in the light of the rapid decay of the internal motion after the detachment of the drop from the nozzle; after this brief time, the drop will be either stagnant or slowly circulating, depending on relative velocity, drop diameter, interfacial tension, and viscosity.

Calderbank and Lochiel (C1a) have recently substantiated Hammerton and Garner's findings (H4) that the rate of transfer does not vary as bubble ages from roughly 1–6 sec after bubble release, over a bubble diameter range of 0.5–2.65 cm. This is in some disagreement with the results of Deindoerfer and Humphrey, obtained with bubbles smaller than 0.5 cm. However, about 45% of the decay of the transfer coefficient reported by the latter workers occurs between 0.5–1.0 sec, which is in general agreement with the more recent studies of Marsh and Heideger.

For suspended bubbles, rigid-drop values were obtained (G21) after some 40–60 sec. Gradual absorption of surface active agents would account for these facts.

The decay of circulation was also reported by Rumscheidt and Mason (R8), who studied internal and external streamlines associated with circulating drops. They showed that behavior inside the drop is highly sensitive to traces of surface active agents present in either fluid phase, and suggested that accumulation of the latter at the interface could render it viscoelastic. Thus the time of complete decay is dependent on the rate at which the surface active impurities are conveyed to the interface (L8, L17). With all surface active agents assumed to be inside the drop, the decay time was found (R8) directly proportional to the velocity gradient and inversely proportional to $(\mu_d/\mu_c) + 1$. However, circulation decay does appear in systems believed to be extremely pure, which is consistent with Henniker's ideas on the viscoelasticity of the interface (H14).

Aging of the transfer coefficients was also noticed by Baird and Davidson (B1) in experiments on absorption of very large CO_2 bubbles in tap water. As suggested earlier by Garner (G12), the unsteady value of the transfer coefficient can probably be attributed to slow saturation of the turbulent wake under the spherical-cup bubble, where transfer is by eddy diffusion rather than by convection. With bubbles less than 2.5 cm diam, time-independent transfer coefficients were obtained. This was attributed (B1) to more rapid bubble circulation and renewal of the wake, which permit a steady state to set in faster behind the smaller bubbles; it is consistent both with the dependence of the steady-state time on the Peclet number (B6), which for spherical bubbles yields $\Theta \propto R$, and with the relationship $\Theta \propto R^{2/3}$, suggested by Levich (L8). However, due to the irregular hydrodynamic

behavior of the "large" spherical-cup bubbles in question, some other factors may be involved. A detailed discussion of some of these factors in relation to gas–liquid mass transfer is given by Calderbank (C1a).

The time dependence of the transfer coefficient is closely related to the observed decrease of the transfer coefficients per unit height with increasing column height (B11, E1, G12, P2), and undoubtedly introduces a significant error in the determination of end effects by the variable-column-height technique.

2. *Transfer Coefficients Outside Circulating Drops*

Internal circulation is generally assumed to cause thinning of the outside boundary layer, thus increasing appreciably the transfer rate between the drop and the ambient fluid (B12, G3). In other words, because of the mobility of the interface, a smaller velocity gradient exists near it that results in larger convective heat transfer. Rumscheidt and Mason (R8) proved the dependence of the streamlines outside and inside spherical drops undergoing laminar shear flow on the viscosity ratio of the fluids. As the exact velocity profiles for normal flow conditions are unknown, the solutions for the transfer rate that account for this effect are only approximate.

Johnson *et al.* (B12) followed Friedlander's (F2) solution based on the Stokes velocity profiles around solid particles, and numerically calculated the external coefficients for $N_{Re} < 1$. Only a slight difference in the Nusselt number was observed when the velocity profiles of Stokes and Hadamard were postulated. These calculations showed that the transfer coefficient ratio of drops and solids increases from 1 for $(N_{Pe})_c = 1$ to 3 for $(N_{Pe})_c = 10^4$. In the absence of oscillation, similar results may be expected at moderately higher Reynolds numbers (C1, H3).

The solution for low Reynolds number (or "creeping" flow), $(N_{Re})_c < 1$, and high Prandtl numbers, i.e., $N_{Pe} \gg 1$, was analytically derived by Levich (L8, p. 404). The approximate streamline is given as

$$\psi = u_s R(r - R) \sin^2 \phi \tag{16}$$

When u_s, the velocity at the drop's equator, is taken as $u\mu_c/2(\mu_c + \mu_d)$, the Nusselt number is

$$(N_{Nu})_c = 0.65(N_{Pe})_c^{0.5}\left(\frac{\mu_c}{\mu_c + \mu_d}\right)^{0.5}; \qquad N_{Pe} \gg 1, \qquad N_{Re} < 1 \tag{17}$$

A similar equation is suggested by Griffith (G21). Experimental confirmation of Eq. (17) is reported (L8). Some other proposed solutions are given in Table III and compared graphically in Fig. 7.

No exact analytical solution for heat transfer to drops at $(N_{Re})_c > 1$ is possible at present. However, some approximate solutions are possible, depending on the degree of motion postulated for the fluid interface. For the Reynolds number range $10 < N_{Re} < 30$ and $N_{Pe} \gg 1$, Hamielec and Johnson

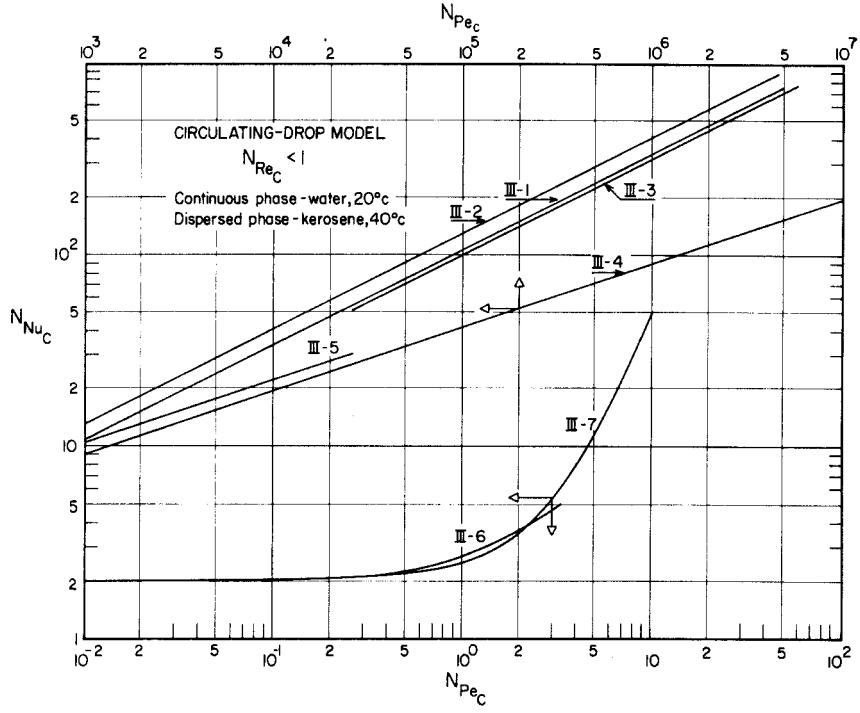

FIG. 7. Comparison of equations for outside Nusselt number (Table III).

(H3) obtained functional approximations for the velocity components by assuming a trial stream function in the Navier–Stokes equations and evaluating the undetermined coefficients from the boundary conditions using the method of residuals. Their relationship can be presented in the form of

$$(N_{Nu})_c = 1.13 f(N_{Pe})^{0.5} \tag{17a}$$

Recurrence formulas related the higher coefficients in the original stream function to their respective first coefficients, and these were given graphically as a function of the Reynolds numbers, up to 30. An extension of this solution to $N_{Re} = 70$ was subsequently given (graphically) by Baird and Hamielec (B1a). Some of the other proposed solutions are summarized in Table III and compared in Fig. 8.

The theoretically simplest approach is to assume that no external boundary layer exists, thus obtaining the highest average values for the external transfer coefficients. Experience proves this assumption to hold for many important practical applications (D8, H8, H13, W3, and others), where the Reynolds number and viscosity ratio μ_c/μ_d are high. Boussinesq (B10) was the first to

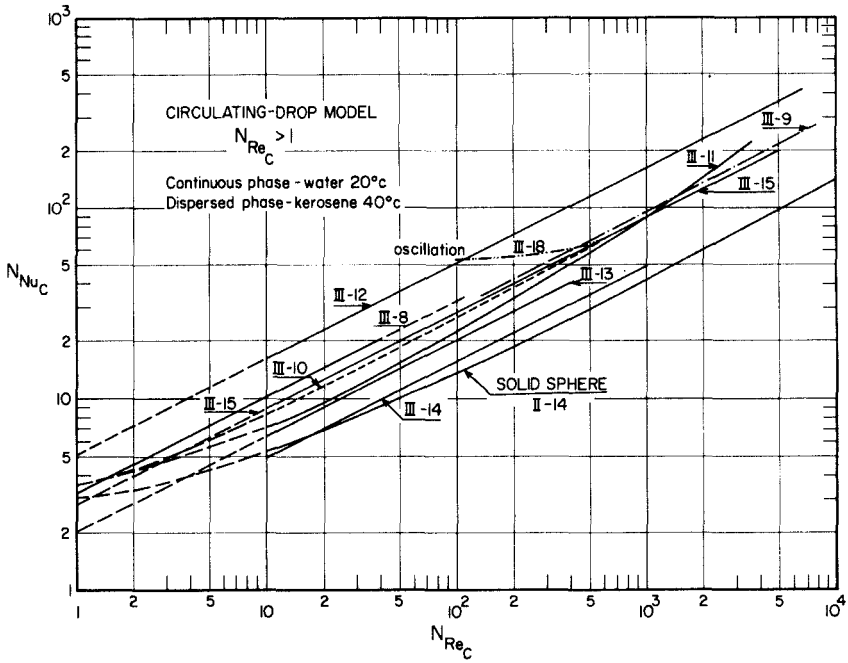

FIG. 8. Comparison of equations for outside Nusselt number (Table III).

apply potential flow in solving forced convection heat transfer and, recently, Ruckenstein (R7) applied it in determining heat-transfer coefficients at the interface of growing vapor bubbles. With certain simplifying assumptions, the well-known equation for steady-state heat transfer is obtained:

$$(N_{Nu})_c = 1.13(N_{Pe})_c^{0.5}; \qquad N_{Pe} \gg 1 \tag{18}$$

By modifying Boussinesq's transformation to allow for unsteady state, the time-dependent temperature distribution in potential flow past a spherical bubble was recently obtained (B6) numerically. For low Peclet numbers ($2 < (N_{Pe})_c < 100$), where the conduction contribution cannot be neglected, graphical integration of the steady-state temperature profiles yields approximately

$$(N_{Nu})_c \simeq 1.25(N_{Pe})_c^{0.5}; \qquad 2 < N_{Pe} < 100 \tag{19}$$

We note that Higbie's penetration theory (H15), with contact time assumed as that required by the drop to traverse a distance of one diameter (W6), gives an expression identical with Eq. (18). Although potential-flow theory, unlike the penetration theory, takes interfacial acceleration into account, the two are actually physically identical, both being based on diffusion into an element of fluid sliding over the constant-temperature interface.

Conkie and Savic (C5) proposed a correction factor for the presence of a boundary layer by introducing a velocity factor K_v defined as the ratio of the true interfacial velocity and potential-theory velocity, and dependent on the Reynolds number and viscosity ratio (Fig. 9). In their view, the boundary

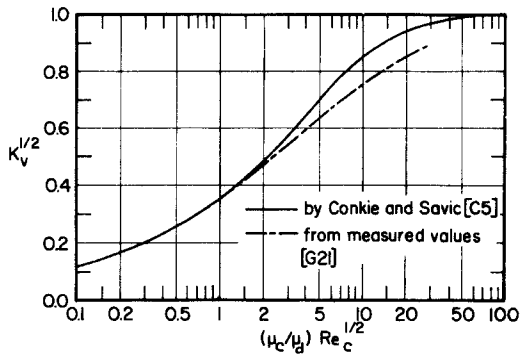

FIG. 9. The ratio K_v of the speed with which the interface between a drop and surrounding fluid moves to that speed with which the interface would move if the fluids were ideal (G21). (Courtesy of *Chemical Engineering Science*.)

layer velocity around the drop varies by a factor of $(1 - K_v)^{0.5}$, with K_v tending to zero at very low Reynolds numbers and to 1 at high Reynolds numbers. Griffith (G20, G21) extended this approach and incorporated the velocity factor in his equations for both slowly and rapidly circulating drops. The suggested equation for rapidly circulating drops is

$$N_{Nu} = 2 + 1.13(N_{Pe})_c \cdot K_v)^{0.5}; \qquad N_{Pe} \gg 1 \tag{20}$$

where the constant "2" was artificially introduced to allow for the lowest theoretical Nusselt number in a stagnant medium. With $K_v = 0.53$, one obtains Eq. (III-14). A basically similar relationship was obtained by Chao (C4a) who applied boundary layer theory to flow around circulating fluid spheres by considering viscous effects as a perturbation on potential flow. Comparison of his expression for the Nusselt number with Eq. (20) yields

$$K_v = 1 - 1.43(N_{Re})_c^{-1/2} \tag{20a}$$

applicable for $100 < (N_{Re})_c < 1000$. A more accurate expression, including

the viscosity ratio, is given by Lochiel and Calderbank (L18):

$$K_v = 1 - \frac{2 + 3\mu_d/\mu_c}{1 + (\rho_d\mu_d/\rho_c\mu_c)^{1/2}} 1.45(N_{Re})_c^{-1/2} \tag{20b}$$

Solutions for the transfer coefficients around axisymmetric bodies of revolution (oblate and prolate spheroids and bubbles with spherical cups shapes) in potential flow were also reported (L18) and related to experiment (C1a).

The maximum possible continuous-phase heat transfer coefficient obtainable for nonoscillating drops was suggested by Elzinga and Banchero (E2). Their equation is based on the maximum heat transfer to a solid sphere, calculated in the vicinity of the front stagnation point. Applying it to drops with internal circulation they obtained

$$(N_{Nu})_c = 1.96(N_{Pe})_c^{0.5} \tag{21}$$

As mentioned previously, Terjesen *et al.* (B13, T3) attribute the high transfer coefficients characterizing circulating drops, in contrast to noncirculating drops, to their relatively higher velocities. Thus circulation is associated with higher drop velocity, and accordingly with higher Reynolds numbers and higher transfer rates. They also showed that the effect of interfacial turbulence (or "interfacial agitation") is rather small compared with that of velocity. The higher coefficients are attributed to hydrodynamic disturbances in the unstable boundary layer and the vortex formed behind the moving drop. Thus, "in contrast to the solid spheres above a certain Reynolds number, most of the transfer takes place at the rear of the drop" where the boundary layer is unstable and undefined, and turbulence exists. Terjesen's data are in good agreement with Garner's equation (III-16) where the exponent of the Prandtl number is 0.42, as well as with his own (III-17) where the exponent is $\frac{1}{3}$; this also indicates that drop viscosity (in the range 0.6–1.7 cP) has very little effect on the external transfer coefficient.

Drop oscillation was found to increase the rate of mass transfer by a factor of two (G9) to four (S13), unlike gas–liquid systems (C6), due probably to reduced external resistance (G12). Oscillation usually sets in at Reynolds numbers between 150 and 200, bringing about a higher power than $\frac{1}{2}$ for the Reynolds number (G12, L13, C7), which is consistent with Eq. (6). Oscillation of the wake, setting in at about the same Reynolds number (200), was found to have a similar effect on the rate of transfer (G12). Oscillation effects are of importance in systems with a low-viscosity continuous phase, where Reynolds numbers higher than 200 are obtained. Oscillation is also stronger in systems with low interfacial tension and low viscosity of the dispersed phase (G12). For circulating and oscillating drops Garner suggests the

following empirical equation:

$$(N_{Nu})_c = 50 + 8.5 \times 10^{-3}(N_{Re})_c{}^{1}(N_{Pr})^{0.7} \tag{22}$$

The maximum deviation of the experimental data in the range of $150 < (N_{Re})_c < 700$ was reported as 12%

3. *Transfer Coefficients Inside Circulating Drops*

The equations of fluid motion inside and outside a circulating drop under viscous flow regime were solved by Hadamard (H2) and Rybczynski (R9) in 1911, and are quoted in hydrodynamics textbooks (L2). The complete derivation is also repeated by Levich (L8). Although Hadamard's stream functions are strictly applicable to the viscous region only, visual observations (G10, S18) indicated that the function approximates actual flows (E2, H3). Hadamard's stream function inside the drop, as given in polar coordinates with the origin at the center of the drop (K5), is

$$\psi = -\frac{g\,\Delta\rho\,R^2}{6(2\mu_c + 3\mu_d)}(1 - r^2)r^2 \sin^2\phi \tag{23}$$

Kronig and Brink (K5) used the Fourier–Poisson equation to derive equations for the temperature distribution and heat transfer inside a drop with internal circulation described by Eq. (23). Assuming that diffusion is negligible along internal streamlines and that the isotherms at any particular moment coincide with the streamlines, and disregarding external film resistance, they obtained the following equation for the transfer efficiency:

$$E_m = 1 - \frac{3}{8}\sum_{n=1}^{\infty} A_n{}^2 \exp\left[-\frac{\lambda_n 16\alpha_d\Theta}{R^2}\right] \tag{24}$$

The constants A_n and eigenvalues λ_n were recalculated more recently by Elzinga and Banchero (E2), who also determined them for various external film resistances. Their data are summarized in Tables A-II and A-III in the Appendix.

Danckwerts (D1) has pointed out that Eq. (24) is not as limited as originally implied; this is evident from many experiments (C1, Table I) with Reynolds numbers up to 2000 under oscillation-free conditions. A simpler empirical equation (Eq. IV-6, Table IV) in close agreement with Eq. (24) was suggested by Calderbank and Korchinski (C1). A graphical comparison of Eq. (24) with Eq. (IV-6) and Eqs. (8)–(10) is shown in Fig. 10. Kronig and Brink's solution gives heat-transfer coefficients about 1.5 times higher than the solid drop model, corresponding to an effective diffusivity 2.25 times larger than the molecular diffusivity. This is to be expected, as their model in effect implies reduction of the drop diameter (by about half) to a size charac-

teristic of the circulation pattern (H5). Since Kronig and Brink's stream lines are closed loops, the transfer rate calculated by Eq. (24) is independent of the circulation velocity.

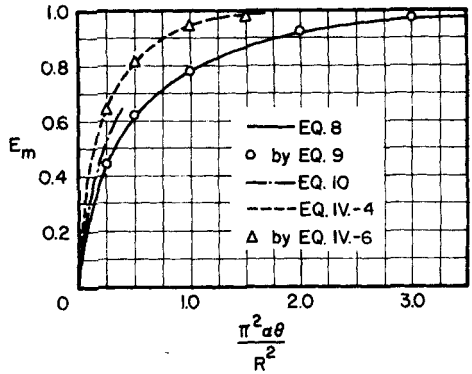

FIG. 10. Equations for diffusion into stagnant and circulating drops (C1).

Handlos and Baron (H5) proposed another model for the more practical range of Reynolds numbers (about 1000). They assumed that the tangential motion caused by circulation is combined with an assumed random radial motion caused by internal vibration, and determined the eddy diffusivity α_e subsequently used in solving the appropriate Fourier–Poisson equations. They postulated radial stream lines, as shown in Fig. 11, rather than those

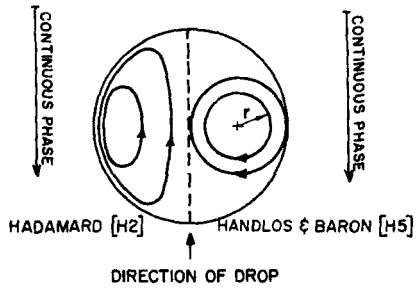

FIG. 11. Comparison of drop-circulating models.

derived by Hadamard. Using probability functions, Kronig and Brink's average circulation time, and Einstein's equation to correct the mean-square deviation for a given time to the effective diffusivity, they obtained

$$\alpha_e = \frac{(N_{Pe'})_d}{2048}(6\omega^2 + 8\omega + 3) \tag{25}$$

where

$$(N_{\mathrm{Pe}'})_d = \frac{(N_{\mathrm{Pe}})_d}{1 + \mu_d/\mu_c} \tag{26}$$

$\omega = 4r/D$, and r is the radial distance from the center of the circulation torus. Using the first eigenvalue only, the transfer efficiency of Eq. (IV-7) is conveniently reduced to

$$E_m \simeq 1 - \exp\left[-5.62 \times 10^{-3}(N_{\mathrm{Pe}'})\frac{\alpha_d \Theta}{R^2}\right] \tag{27}$$

The internal Nusselt number is given (H5) by

$$(N_{\mathrm{Nu}})_d = 0.00375(N_{\mathrm{Pe}'})_d \tag{28}$$

Their experimental data are in agreement with the theoretical values within 20%. Extension of Handlos and Baron's model to include surface resistance was recently proposed by Welleck and Skelland (W4a).

If potential flow and constant surface temperature are assumed, an equation analogous to Eq. (18) is obtained for the internal Nusselt number. Note, however, that the reference velocity in the internal Peclet number is the drop velocity. Similar results will be obtained from the penetration theory, according to which the film is assumed infinite with respect to the depth of heat penetration during the short contact time of a fluid element "sliding" over the interface. Licht and Pansing (L13) report West's equation, based on the transient film concept, for the case of mass transfer through the combined film resistance. In terms of the overall heat-transfer resistance, $1/U$ $(= 1/h_d + 1/h_c)$ and if the contact time is that required for the drop to traverse a distance equal to its diameter, West's equations yield

$$E_m = 1 - \exp\left[-3.39\left(\frac{\alpha_U \Theta}{R^2}\right)^{0.5}\right] \tag{29}$$

where

$$\alpha_U^{1/2} = \frac{(\alpha_c \alpha_d)^{1/2}}{\alpha_c^{1/2} + \alpha_d^{1/2}}$$

For negligible drop-side film resistance, $U = h_c$, $\alpha_c/\alpha_d \ll 1$, and $\alpha_U^{1/2}$ approaches $\alpha_c^{1/2}$. For negligible continuous side film resistance, $U = h_d$, $\alpha_c/\alpha_d \gg 1$, and $\alpha_U^{1/2}$ approaches $\alpha_d^{1/2}$.

An experimentally convenient technique for relating internal transfer coefficients is based on applying an experimental factor $\bar{R}$, the effective diffusivity factor, to the rigid-drop equations. $\bar{R}$ is the ratio of effective and molecular diffusivity in a stagnant drop. Equation (IV-8), in effect, defines the $\bar{R}$ factor. $\bar{R}$ ranges from 1.6 to 3.3 circulating drops at moderate Reynolds

numbers and up to 70 for moderate and high Reynolds numbers, in the presence of drop oscillations (C1).

The experimental effective diffusivity factor should normally approach the value of 2.25 calculated by Kronig and Brink (K5) at low Reynolds numbers. For drops with "turbulent" circulation described by Handlos and Baron's model, $\bar{R}$ is given (J2) by

$$\bar{R} = (N_{\mathrm{Pe}'})_d/2048 \tag{30}$$

In practice, lower values than those calculated according to Eq. (30) are found for intermediate Reynolds numbers, only approaching them in the presence of oscillation. A compilation of experimental $\bar{R}$ factors is available (C1). The experimental effective diffusivity in gas absorption with internal circulation has been plotted against the axial velocity representing the flow adjacent to the interface (G7), and shows a direct relation between circulation and internal resistance. Similar results are reported (C6) for other gas-liquid and liquid–liquid systems.

Constan and Calvert (C6) recently proposed a theoretical equation for the effective diffusivity, as a function of the transfer efficiency and of a pseudo-film-thickness dependent on circulation velocity. However, no correlation between the film thickness and the Reynolds number yet exists. Use of this theoretical equation necessitates measurement of the circulation velocity, which does not simplify matters.

The various equations derived for the transfer efficiency are summarized in Table IV. The equations for the rigid-drop model are included for comparison.

IV. Heat Transfer to Drops Moving in a Continuously Varying Temperature Field

A. Single-Drop Studies

Compared with the large volume of work dealing with drops at constant temperature (or concentration), very little has been reported on single drops moving in a variable temperature (or concentration) medium. A variable temperature, with an approximately linear temperature gradient, was used by Wakeshima (W1, W2), to study the limit of superheat of pure liquid drops. However, since drop temperature could not be measured, his data cannot be used for determination of heat-transfer coefficients.

An interesting study on the effect of continuous longitudinal temperature gradient at the surface of a droplet on its flow characteristics is given by Young *et al.* (Y1). Under these conditions, droplets (and bubbles) were shown

to move in the direction of their warmer poles. "Small bubbles are attracted by hot objects."

The internal heat-transfer efficiency for a rigid drop with zero external film resistance, moving at a constant velocity in a fluid under linear temperature change along the drop path, can be shown (C4) to be

$$E_m = 1 - \frac{R^2}{\alpha\Theta}\left(\frac{1}{15} - \frac{6}{\pi^4}\sum_{n=1}^{\infty}\frac{1}{n^4}\exp\left[-\frac{n^2\pi^2\alpha\Theta}{R^2}\right)\right] \tag{31}$$

For a rigid drop (with a finite external film resistance) moving in an arbitrary but continuous temperature field of the continuous phase, following Barbouteau's (B3) model, the internal heat-transfer efficiency (S8) was found to be

$$\bar{E}_m = \frac{T_0 - T_i}{T_{c0} - T_i} = -\frac{2}{3(B-1)} - 6\sum_{n=1}^{\infty} C_n \exp[-\lambda_n^2 SZ/R] \tag{32}$$

where T_{c0} is the average temperature of the continuous phase at its outlet (or at the same cross section where T_i, the inlet drop temperature, is measured), Z the column height (or distance traversed by the drop), and

$$S = \frac{\alpha_d}{UR} = \frac{1}{(N_{Pe})_d}, \qquad B = (GC_p\rho)_d/(GC_p\rho)_c,$$

$$C_n = [(3B + E\lambda_n^2)^2 + \lambda_n^2(1 - E) - 9B]^{-1}$$

The eigenvalues λ_n may be calculated from

$$\tan \lambda_n = \frac{3B + E\lambda_n^2}{3B + (E-1)\lambda_n^2} \cdot \lambda_n$$

where

$$E = \frac{k_d}{h_c R} = \frac{1}{N_{Bi}}$$

The continuous-phase temperature T_{cz} at any cross section of the column may be determined from the following equation:

$$\frac{T_{cz} - T_{c0}}{T_{c0} - T_i} = 6B\sum_{n=1}^{\infty} C_n[1 - \exp(-\lambda_n^2 SZ/R)] \tag{33}$$

For gas oil dispersed in water, with the external film-transfer coefficient taken as 25 Btu/hr/ft^2/°F, the first two eigenvalues are $\lambda_1 = 2.07$ and $\lambda_2 = 2.07 + \pi$ (B3).

In spite of the reported agreement of the derived equation with experimental data of a gas–oil–water spray column (B3), modification for actual spray columns is indicated. Actual velocities and contact areas per unit volume are functions of the dispersed phase holdup and should replace the

single-drop terminal velocity and contact area used in the above derivation. Also, Elgin's (B7, W4) rather than Hayworth's (H12) correlation for drop diameter seems advantageous (L5).

B. Countercurrent Spray-Column Heat Exchangers

High liquid throughputs, large contact area per unit equipment volume, and relatively inexpensive operation as well as relatively low equipment costs encourage the use of countercurrent spray columns as direct-contact heat exchangers. Spray columns are almost as efficient as packed columns, when one is working with systems of low interfacial tension, due to the small drops formed. For work with high-surface-tension systems, packed beds are considerably more efficient (S17), although their operation is usually more expensive compared with spray columns. A schematic diagram of a spray column is shown in Fig. 12.

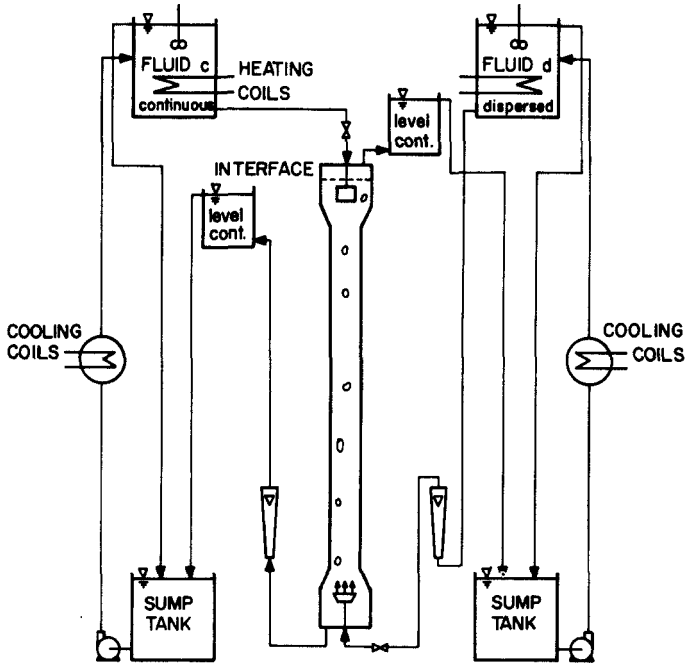

FIG. 12. Schematic diagram of spray column.

The numerous variables involved in spray-column exchangers have hitherto defied even approximate engineering correlation. Collation and adaptation of the information and experience accumulated in mass-transfer

and fluidization studies is highly desirable. Also, further basic experimental studies under closely controlled conditions are needed to determine interrelationships of the various factors affecting the flow characteristics as well as the heat-transfer phenomena. Nevertheless, in spite of certain reservations and contradictory evidence, some important general characteristics emerge to guide future applications of this promising mode of heat transfer.

Heat-transfer data are normally reported in terms of the volumetric heat-transfer coefficients, defined as

$$U_v = \frac{q}{V(\Delta T)_{\ln}} \tag{34}$$

where q is the amount of heat transferred between the phases in the column per unit time, V the total column volume, and $(\Delta T)_{\ln}$ the log-mean average of the measured temperature differences between the two phases at the inlet and outlet. Some workers use the plate or transfer unit, HTU. For the continuous phase the relationship between the volumetric heat transfer coefficient and the apparent height of the transfer unit, based on the over-all resistance to transfer between the phases HTU_{0c}, is given by

$$HTU_{0c} = \frac{(GC_p\rho)_c}{U_v} = Z\left(\int_{Tc_1}^{Tc_2} \frac{dT_c}{T_c - T_d}\right)^{-1} \tag{35}$$

where G_c is the superficial velocity of the continuous phase.

For spherical drops, the total transfer area per unit column volume is given by

$$\frac{A}{V} = \frac{6F}{D}$$

where F is the holdup ratio, i.e., the ratio of the dispersed phase volume and the total volume of the column. Thus the obvious relation between the volumetric and the surface heat-transfer coefficients is

$$U_v = \frac{6F}{D} U \tag{36}$$

As is expected intuitively, the surface heat-transfer coefficient decreases with increasing dispersed-phase holdup (G13). This is probably due to the impeded flow characteristics, decreasing internal circulation and possible obstruction of the interfacial area by closely packed drops. Under normal operating conditions (up to the flooding point) the increase of A/V is appreciably larger than the decrease of U with F. Denser packing and therefore higher holdups yield higher volumetric heat-transfer coefficients.

Sakiadis and Johnson (S1) have proposed a general equation for flooding rates. With water as the continuous phase ($\mu = 1$ cP) their equation for the

dispersed-phase superficial velocity reduces (T2) to

$$G_d \simeq \frac{1.1(Dg\,\Delta\rho)^{1/2}}{1 + 3.6(\rho_d/\rho_c)^{1/4}(G_d/G_c)^{1/2} + 3.24(\rho_d/\rho_c)^{1/2}(G_d/G_c)} \tag{37}$$

where D is measured in feet and $g = 4.17 \times 10^8$ ft/hr^2.

The column should operate at maximum efficiency when the transfer coefficient is infinite, or else when the temperature gradient is the same for the two ends (or two phases). Thompson *et al.* (T2) suggested that the ratio $(\Delta T)_d/(\Delta T)_c = 1$; hence, one should use

$$(G_d/G_c) = (C_p\rho)_c/(C_p\rho)_d \tag{38}$$

to obtain highest operating efficiency. They proposed an elaborate column design procedure which takes into account the change of heat capacity with temperature, in the column.

In general, at any given dispersed phase flow rate, the volumetric heat-transfer coefficient is only slightly affected by the continuous-phase flow rate. However, since holdup, flooding, and volumetric transfer coefficients are functions of the flow rate ratio (G_d/G_c), different continuous-phase rates give different flooding conditions resulting in different values for the maximum volumetric coefficients. Once "optimal" ("near-flooding") conditions are reached, an increase of the dispersed-phase flow rate will cause larger drops to be formed and coalescence to set in, thus drastically reducing the transfer coefficients. It is therefore expected that the transfer coefficients should be some function of the flow ratio or the holdup, for any given system, and this indeed has been found experimentally.

The relationship between holdup and slip (relative) velocity between the two phases is, by definition,

$$V_s = \frac{G_c}{1 - F} + \frac{G_d}{F} \tag{39}$$

The slip velocity applies strictly when the two phases are in plug flow; higher slip velocities may be encountered, in practice, under nonideal flow conditions.

Relations between slip velocity, holdup, and drop diameter, from the data of Letan and Kehat (L5) for a 3-in. column (kerosene-water system), are illustrated in Fig. 13. The increase in drop diameter with increasing holdup and decreasing slip velocity has some effect on the transfer area per unit volume, which nevertheless increases with decreasing V_s. Volumetric transfer coefficients increase correspondingly.

It is evident from Fig. 13 that, as flooding (or rather "near flooding") is approached, the drop diameter for a given fluid system is then a function of flow rates, holdup, and temperature, rather than of the orifice diameter.[3]

[3] Holdup is independent of orifice diameter, but dependent on dispersed-phase flow rate [Q1].

This case is thus in agreement with the findings of Thompson *et al.* (T2), that for a given two-fluid system "heat transfer is practically independent of orifice diameter." This conclusion, though it may apply for the 0.04- to 0.064-in. nozzles tested by Thompson *et al.*, is subject to reservation for larger diameters. The extensive study of Minard and Johnson (M5) reveals a relatively small but appreciable effect of nozzle diameter over the range from 0.04 to 0.86 in.

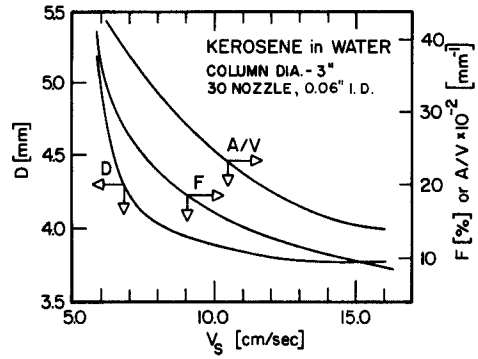

FIG. 13. Relationship between drop diameter, holdup, volumetric heat-transfer area, and slip velocity.

Spray-column heat exchange work is summarized in Table V. A brief review of these studies, with some general conclusions, follows. Some of the data for benzene, toluene, and water systems are compared in Fig. 14.

Garwin and Smith (G13) undertook an extensive study of a spray column with benzene dispersed in water, and determined overall heat-transfer coefficients as a function of holdup and phase velocity. Drop size was found to be independent of the water flow rate, and predictable by means of Hayworth and Treybal's equation (H12). However, this may not be true near the flooding point, where relatively few runs were made. The volumetric heat-transfer coefficient increased moderately with increasing water flow rate (except at the high benzene flow rates, where the observed increase was very high) and with benzene flow ratio and holdup. Statistical treatment of their results (T2) yields

$$U_v = 1.09 \times 10^4 F \qquad \text{(hot water to benzene)} \tag{40}$$

$$U_v = 1.67 \times 10^4 F \qquad \text{(hot benzene to water)} \tag{41}$$

where U_v is in Btu/hr/ft^3/°F. The average drop diameter was 7.34 mm for hot-water runs, and 6.71 mm for hot-benzene runs; this difference accounts only partially for the difference in volumetric transfer coefficient, which is inversely proportional to the drop diameter (T2).

Rosenthal's earlier work (R5) with toluene dispersed in water is reported by Treybal (T6) as a plot of HTU_{0c} vs (G_d/G_c), yielding, for thirteen nozzles each 0.281 in. i.d.,

$$HTU_{0c} = 6.2(G_c/G_d)^{1.04}; \quad \text{or} \quad U_v = 4.28G^{1.17}(G_d/G_c)^{1.13} \tag{42}$$

and for 71 nozzles each 0.120 in. i.d.,

$$HTU_{0c} = 4.4(G_c/G_d)^{1.15}; \quad \text{or} \quad U_v = 5.25G^{1.17}(G_d/G_c)^{1.13} \tag{43}$$

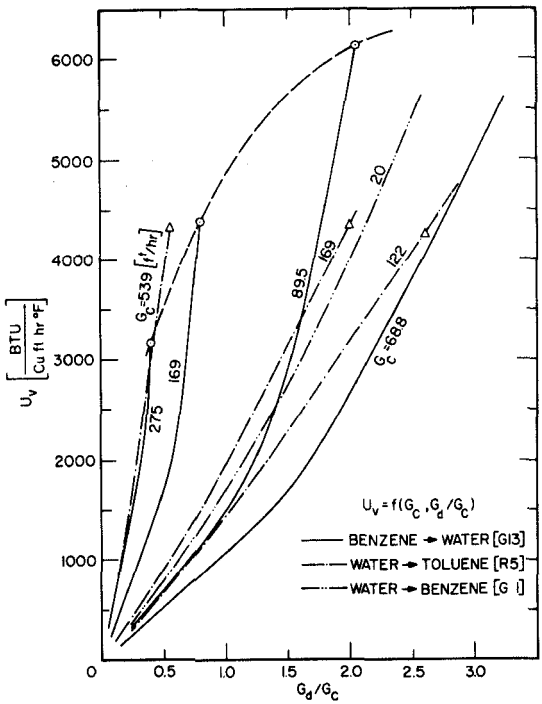

FIG. 14. Comparison of some spray-column heat-exchanger data.

The overall volumetric transfer coefficient is apparently independent of the continuous-phase flow rate over the range investigated.* The ratio $G_d/G_c = 2.87$ is recommended (T2) for maximum efficiency of this system.

Woodward (W12, T2) studied the operation of single, sectionalized, and double-column exchangers. Shell Fluid A and Shell Deodorized Spray Base were dispersed in water and in sea water. Data reported for the Fluid A–water system in a single column are summarized in Table V. From these, the dependence of the overall heat-transfer coefficient on dispersed-phase holdup

* Similar results were recently reported for six perforated plate-column (S0) (In press).

is approximately

$$U_v \simeq 1.2 \times 10^4 F \tag{44}$$

for $(G_d/G_c) = 2.5$, the maximum efficiency ratio for the system.

No appreciable effect of column height (5 ft 4 in. to 8 ft 8 in.) on the transfer coefficient was noticed. Sea water and fresh water gave similar results. Contrary to Garwin's experience, the heat-transfer coefficients were found to be larger when the top of the column was hot than when the top was cold. With $G_d/G_c = 2.58$ and $F = 0.6$, values of 8180 and 7030 Btu/ft^3/hr/°F for hot and cold top, respectively, were obtained with spray base as the dispersed phase. The maximum values of the volumetric heat-transfer coefficient were 11,500 and 8500 Btu/ft^3/hr/°F for the hot and cold top, respectively. These results probably reflect the natural convection currents in the column as well as with the very pronounced effect of fluidity of the oil on the volumetric heat-transfer coefficient (W12, Fig. 12). Since Garwin worked with benzene, it is likely that this fluidity effect would have been relatively less pronounced in his experiments.

The question of the effect of direction of heat flow between the phases on the transfer coefficients is intriguing. Evidently the results obtained are subject to at least three different effects, possibly mutually counteractive. These are internal natural convection, over-all natural convection currents in the column, and temperature effects on the properties affecting the local transfer coefficient. Johnson *et al.* (J3) worked with the heavy phase (carbon tetrachloride) as the dispersed phase, and found the heat-transfer coefficient to be higher when the dispersed phase was the hot one; this result is attributed by Johnson to the temperature effect on the boundary layer surrounding the drop. There is no contradiction, however, between Johnson's and Woodward's results, if the direction of heat flow in the towers, rather than between the phases, is considered. In both studies, higher transfer coefficients were found when the top of the column was hot, indicating a better transfer coefficient when the towers operate in their natural heat-flow direction. Reverse operation would most probably increase backmixing due to natural convection currents in the column. The larger differences in transfer coefficient for the two arrangements in Johnson's work, as compared with Woodward's, seem to indicate the existence of a small additional effect of the direction of heat flow as between the dispersed and continuous phase.

Because of his relatively larger differences in drop diameter, Garwin's results cannot be properly considered here. They conform with the concept that internal natural convection currents enhance the mobility of the interface which nevertheless fail in the light of Johnson's as well as Woodward's experimental results. The question is obviously open, and the need for controlled experiments under identical temperature and flow conditions is indicated. The theoretical study of Young *et al.* (Y1) on the motion of bubbles

TABLE V COMPARISON OF SO

No.	Dispersed phase, d	Continuous phase, c	Direction of transfer	Column		Nozzles		G_c ($ft^3/hr/ft$
				Diameter	Height	No.	i.d. (in.)	
1	Benzene	Water	$d \rightarrow c$ $c \rightarrow d$	2″	6′	20 (?)	0.125	65–27
2	Toluene	Water	$c \rightarrow d$	5.375″	10′ 9″	13 71	0.281 0.12	147–59 122–53
3	CCl_4	Water	$c \rightarrow d$ $d \rightarrow c$	4″	8′	21	0.228	93–64 93–61
4	Shell Oil A	Water	$c \rightarrow d$	4″	5′ 8.5″	189	0.064	65–76
	Shell Oil A[a] Spray base	Water Sea water	$c \rightarrow d$ $d \rightarrow c$	4″	5′ 4″–8′ 8″	104–450	0.0625–0.04	40–86
	Spray base	Water	$c \rightarrow d$ $d \rightarrow c$	4″	6′	450 204	0.04 0.064	52 52
5	Gas-oil	Water	$d \rightarrow c$	1′ 3.7″	13′ 1″	70	0.315	52–18
6	Kerosene	Water	$d \rightarrow c$	3″	6′ 11″	30	0.06	45–16
7	Mercury	Water	$d \rightarrow c$	1″ 2″	1′ 1.25″ 1′ 7.375″	73–1 113–9	0.0225–0.189	295–88 148
8	Benzene	Water	$c \rightarrow d$	2″	$\frac{1' 6''}{8}$[b]	62 × 8[b]	0.127	20

[a] Also Aeroshell Turbine Oil and AMSCO Odorless Solvent (T2).
[b] 8 sieve-plates in column.

or droplets in a vertical temperature gradient due to surface stresses should also be considered in this connection.

The study of Pierce, Dwyer, and Martin (P3) on heat transfer and fluid dynamics in mercury-water spray columns serves to illustrate some of the factors which may greatly reduce the efficiency of spray-column operation. Backmixing was observed at the water inlet region, and water bypassed the stream of mercury drops in the column, resulting in two countercurrent streams of water flowing inside the column. This greatly increased the water temperature in the water-inlet region, and reduced the allowed temperature gradient in the column. The heat-transfer coefficients per unit area were thus found to be smaller than those calculated for stationary rigid spheres in a flowing constant-temperature medium. However, the differences between calculated and experimental values decrease with increasing Reynolds number from ten-to-one ratio (20/2) of the Nusselt number at $(N_{Re})_c = 500$ to a 1.5 ratio (45/30) at $(N_{Re})_c = 3000$. Experiments were conducted at

RAY-COLUMN HEAT-TRANSFER STUDIES

G_d ft³/hr/ft²)	F (Holdup)	U (Btu/ft³/hr/°F)	$U_v \times 10^{-3}$ (Btu/ft³/hr/°F)	HTU_{oc} (ft)	Source
45–185	0.08–0.74 0.04–0.36	40–70 30–50	1–6.5 0.4–4	—	Garvin and Smith (G13)
43–260 60–317	<0.275< —	—	1.3–5.6 1.2–6.3	2.5–70 1.5–40	Rosenthal (R5, T6)
32–250 32–250	Max	—	0.1–0.75 0.1–1.08	—	Johnson *et al.* (J3)
160–186	0.20–0.56		2.7–6.0		
118–202	0.48–0.72	—	5.9–11.5 5.2–8.5	—	Woodward (W12) Thompson *et al.* (T2)
135	0.60		8.18		
135	0.60		7.03		
52–204	?	14–34	0.26–1.26	—	Barbouteau (B3)
110–240	0.20–0.35	20–50	0.5–7.0	—	Letan and Kehat (L5)
140–355 64–100	0.025–0.07 0.007–0.011	400–1170 520–760	16–48 8.1–12.7	—	Pierce (P3)
16–66	0.13–0.40	30–60	1.5–5.7	0.2–0.8	Gardner (G1)

numerous combinations of column diameter and length, and number and diameter of nozzles, without yielding any general correlation. The effects of water flow rates, column diameter, height of top calming section, and mixing in the top section appear slight; variation of the volumetric heat-transfer coefficient with drop size were found to be less than expected due to increased mercury surface area. However, the transfer coefficients for a 19-in. column were found to be about 20% lower than those for a 13-in. column, demonstrating the peculiarity of the flow patterns in this experimental system.

Backmixing or longitudinal dispersion of either phase reduces the transfer efficiency in the column. A theoretical study involving a numerical solution with efficiency related to backmixing, was presented by Sleicher (S16). A comprehensive study of some general and specific cases of longitudinal dispersion was recently reported by Miyauchi and Vermeulen (M6). Analytical solutions and graphs are presented (M6) relating the various parameters affecting this phenomenon. In practice, backmixing is mainly associated with the continuous phase and increases with the decrease of the latter's flow rate. Backmixing is especially pronounced in the continuous-phase inlet region

and was found (G14) to be almost independent of continuous-phase inlet nozzle and column design. In general, the denser the packing of the dispersed phase and the higher the flow rates in the column, the lower the effect of backmixing and the higher the rates of heat transfer. Swirling motion of the dispersed phase at the inlet region of the latter was also noted (F1) when operating near the flooding point. For additional details see Section VI,A.

The operation of an industrial-size gas–oil–water spray column (13 ft high, 1.3 ft diam) was reported by Barbouteau (B3). The relatively low overall heat-transfer coefficients calculated from his data, up to 1250 Btu/ft^3/hr/°F, seems to suggest operation at relatively low holdup. Umano (U1) studied spray column in the course of his work on direct-contact freezing units for water desalination.

Li (L10) and Gardner (G1) studied the effects of pulsation and of log-mean temperature gradient on heat transfer between benzene and water, in an eight-plate pulsed column. Their data do not reveal any advantage of a multiplate column over the conventional single-plate one. No effect of pulsation was noticed up to pulsating rates of 600 ft/hr, above which the transfer coefficients decreased appreciably. This contradicts the results obtained in mass-transfer studies, where better transfer coefficients are obtained through pulsation. It is of interest to note that a slight increase occurred in the surface transfer coefficients with increasing dispersed-phase flow rate; this may be attributed to increased agitation and oscillation of the drops in the multiplate column.

Dispersed-phase holdup, and hence the volumetric heat-transfer coefficient, is greatly affected by the presence of physical impurities. Recent experiments carried out in these laboratories (L5), with kerosene dispersed in water, elucidated the effect of dirt and scale which accumulate at the upper oil-water interface. This foreign matter greatly increases the rate of dispersed-phase coalescence at the dirty interface, and inhibits dense packing of droplets, thus greatly reducing the dispersed-phase holdup. With water flowing at a rate of 3.2 ft^3/hr/ft^2 and kerosene at a rate of 7.0 ft^3/hr/ft^2, the volumetric transfer coefficients for clean and dirty interfaces were 4800 and 1800 Btu/ft^3/hr/°F, respectively. The presence of scale may explain the relatively low transfer coefficients obtained by Barbouteau (B3), who used similar fluids in his large-scale experiments. Continuous removal of the sludge from the upper interface is required to eliminate this effect (T2).

C. Cocurrent Heat Exchangers

The related studies on direct-contact cocurrent heat transfer are of practical interest. Grover and Knudsen (G25) determined the rate of heat transfer between a petroleum solvent and water, using a pipe of 8-ft length and 1.5-in. i.d. Three methods of solvent injection were compared; better dispersion

TABLE VI

COCURRENT PIPE HEAT EXCHANGERS

Dispersed phase	Continuous phase	Pipe		W_d (lb/hr)	W_c (lb/hr)	$G_T' \times 10^{-6}$ (lb/hr/ft^2)	$U_v \times 10^{-3}$ (Btu/hr/ft^3/°F)	Source
		Length (ft.)	Diameter (in.)					
Petroleum solvent	Water	8	1.5	1470–3100	900–7300	0.2–0.8	5–50	Grover and Knudsen (G25)
Water	Aroclor	15	3	—	—	1.5–2	15–50	Wilke *et al.* (W10)
Water	Oil[a]	4.5–11.2	0.3–3	—	—	1.4–5.5	20–250	Porter (P5)

[a] 90 Neutral oil.

gave higher volumetric transfer coefficients, showing the latter to be a function of the total mass flow rate of the liquid. For a perforated injector, with flow rate ratios $0.27 < G_d/G_c < 5$, the relation is

$$U_v = 1.115 \times 10^{-3} G_T'^{1.26} \tag{45}$$

where G_T' is the total mass flow rate in lb/hr/ft^2. Values ranging from 5000 to 50,000 Btu/hr/ft^3/°F were obtained for total mass flow rates of 0.2–0.8 $\times$ 10^6 lb/hr/ft^2 (2500–10,000 lb/hr). As one might expect, higher values were calculated for the mixing section only, which was about 3.74 ft long.

Similar experiments were reported by Wilke *et al.* (W10) who studied water injected into Aroclor in a 15-ft 3-in. pipe. Wilke's data also do not indicate any effect of temperature and physical properties on the volumetric transfer coefficients, and can be correlated in terms of the total mass flow rate, namely,

$$U_v = 2.38 \times 10^{-23} G_T'^{4.336} \tag{46}$$

Values in the range of 15,000–50,000 Btu/hr/ft^3/°F were found for flow rates ranging from 1.5 to about 2 $\times$ 10^6 lb/hr/ft^2 (73,000–90,000 lb/hr). However, more recent data for turbulent oil-water pipe flow (P5), is in general agreement with Grover and Knudsen's data for the mixing section. Temperatures of the two liquids in the pipe were obtained by monitoring the output of fine thermocouples on a very fast response recorder. Effects of volume fraction, velocity, pipe diameter, interfacial tension, and viscosity on U_v are reported (P6). General comparison of available data is given in Table VI.

Pipe exchangers seem to give higher volumetric transfer coefficients than spray columns, mainly because of better atomization of the dispersed phase, which yields appreciably higher transfer areas per unit equipment volume. Adaption of the cocurrent mixer-settler type contactor for heat transfer between immiscible liquids has recently been suggested (H5a). By using two such liquid–liquid contactors and a third immiscible fluid as the transfer agent, as shown in Fig. 15(a,b) heat can be similarly transferred between two miscible fluids, flowing countercurrently to each other. However, this mode of operation is associated with emulsion formation, contamination, and some losses, and large settling equipment may be required. In practice, economic consideration should guide the choice between parallel-flow and countercurrent exchangers.

V. Heat Transfer to Drops and Bubbles with Simultaneous Change of Phase

Work on direct-contact heat exchangers was stimulated in the last decade by the quest for economic water-desalination units. Multiphase exchange,

where latent heat is transferred between the immiscible fluids, has been effectively used in direct-contact freezing units in which a dispersed volatile fluid evaporates in the saline water with simultaneous freezing of part of the water. The leaving vapors are then brought in contact with the withdrawn ice in another unit where condensation and melting occurs simultaneously (Fig. 15c).

In addition to the advantages seen in the two-phase liquid–liquid exchangers, utilization of a secondary refrigerant as a transfer agent in the direct-contact multiphase exchangers permits (S12): (a) an economical closed refrigeration cycle; (b) smaller quantities and lower flow rates of the cooling liquid; (c) larger, more effective, heat transfer areas; (d) convenient separation of the fluids in contact; (e) higher (by an order of magnitude) heat-transfer coefficients; (f) lower corrosion due to lower working temperatures. Some technical as well as economical aspects regarding the utilization of these multiphase exchangers were reported by Umano (U2), Weigandt (W8, W9), and others (K1).

Unlike the multiphase exchangers where both the dispersed phase and the continuous fluid medium undergo change of phase, three-phase exchangers may be used for heat transfer at various temperature levels. The latter depends on the choice of the transfer fluid. Stagewise operation of three-phase exchangers in a closed evaporation and condensation cycle was recently proposed by Harriott and Weigandt (H10a) for simultaneous cooling and heating of sea water and desalined water streams flowing countercurrently (Fig. 15d).

A variation of the closed refrigeration cycle was suggested by Wilke *et al.* (W10), who studied evaporation of water from sea water flowing in direct-contact cocurrent flow with hot Aroclor in an horizontal 3-in. pipe. The water vapors were then condensed by direct contact with cold Aroclor in a packed bed column. The reported volumetric heat-transfer coefficients for the boiling section were two to three times higher than those shown in Table VI for the nonboiling section.

A general scheme for utilizing flash evaporation of a secondary refrigerant in water conversion by liquid–liquid water extraction from saline water was outlined recently (C3).

A combination of flash evaporators, direct-contact condensers, and liquid–liquid exchangers has been described by Othmer (O1). In this process water vapors, produced in a multistage flash distillation of heated sea water at successively reducing pressures, are condensed by direct contact with a recycle steam of product water. The heat is from the hot product water and is recovered by an immiscible petroleum oil in one spray column and transferred to the incoming sea water feed in a second spray column.

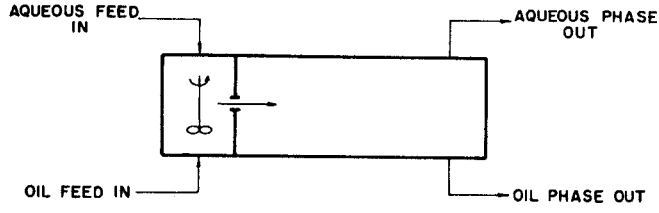

(a)

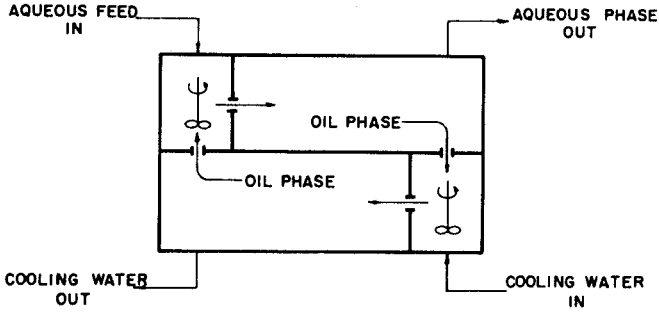

(b)

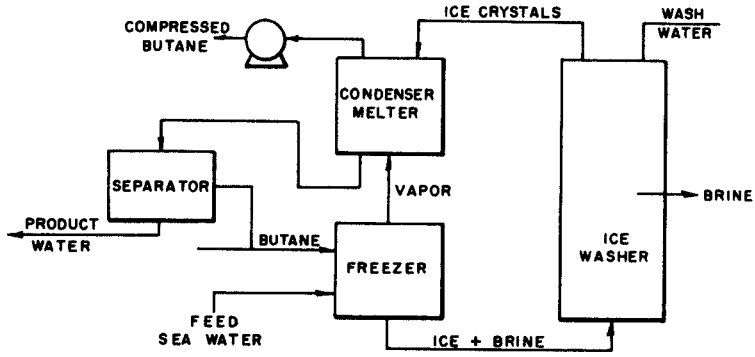

(c)

FIG. 15(a). Direct-contact heat exchangers using mixer-settler contactors for immiscible liquids, after (H5a). (b). Direct-contact heat exchangers using mixer-settler contactors for miscible liquids using a third immiscible liquid, after (H5a). (c). Schematic diagram

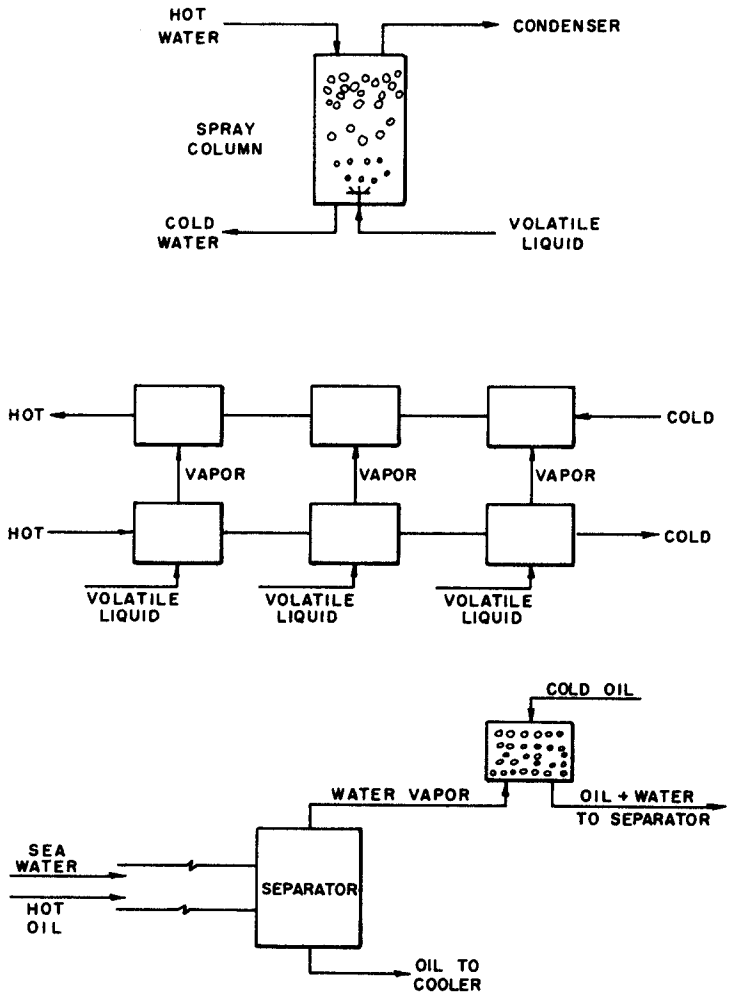

(d)

of multiphase exchangers in direct-contact freezing process. (d). Schematic diagrams of three-phase exchangers: top—single-stage countercurrent spray column; center—countercurrent exchangers in stages; bottom—pipe evaporator and packed bed condenser.

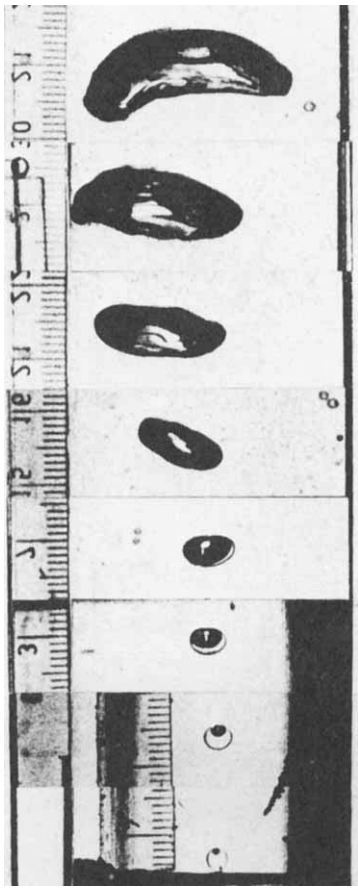

FIG. 16. Pentane drop evaporating in water (S12).

A. EVAPORATION OF DROPS IN IMMISCIBLE LIQUID MEDIA

Although some general technical information on direct-contact heat transfer with change of phase is available, little is known regarding the basic mechanism and heat transfer coefficients encountered when a drop of a volatile fluid evaporates while moving in an immiscible liquid. By means of cinecamera studies of single butane and pentane drops evaporating in stagnant water, Sideman and Taitel (S12) have shown that the vapor concentrates at the upper part of the drop, while the remaining volatile liquid concentrates at the bottom part of the spheroid-like drop. Figure 16 shows a pentane drop evaporating in water at various evaporation ratios. Obviously.

the flow characteristics of the two-phase drop approaches that of a gas bubble as evaporation progresses. Assuming the two-phase drop to be a sphere of constant radius moving in a potential flow field and the volatile liquid at a constant (boiling) temperature, i.e., outside film controlling, the authors obtained an analytical solution for the steady-state heat transfer (S12). Local and average heat transfer coefficients were determined as a function of the opening angle of the vapor phase. The average Nusselt number was found to be

$$(N_{Nu})_c = \left(\frac{3\cos\beta - \cos^3\beta + 2}{\pi}\right)^{0.5} (N_{Pe})_c^{0.5} = C(N_{Pe})_c^{0.5} \qquad (47)$$

where β is equivalent opening half-angle of the vapor phase in the two-phase "drop." Based on experimental data it is suggested that, for $\beta = 135°$, or $C = 0.27$, the maximum average heat transfer coefficient per unit of overall drop area will be obtained. As is to be expected, the Nusselt number decreases with increasing β. For $\beta = 0$, Eq. (47) reduces to Eq. (18), the well-known equation of Boussinesq and Higbie for flow past a sphere.

The overall heat-transfer coefficient, related to the instantaneous total area of the rising two-phase drop, increases sharply with evaporation up to 3–10 wt-% vapor content, depending on the system and conditions, and then decreases quite moderately until evaporation is complete. Thus it indicates the decreasing effect of the internal resistance to heat transfer in the first stages of the evaporation process, and the moderate decrease in the relative transfer area in the subsequent stages of the process (S12). The instantaneous overall heat-transfer coefficients are 200–400 Btu/hr/ft^2/°F for $D^* = 3.5$ mm, and 500–700 Btu/hr/ft^2/°F for $D^* = 2.0$ mm.

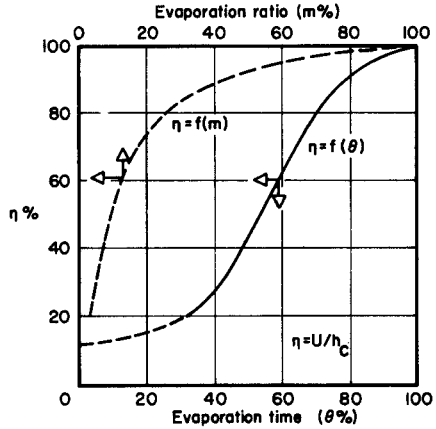

FIG. 17. External resistance controlling factor—pentane drop evaporating in water (S10).

Approximate calculations of the relative importance of the internal and external resistance to transfer in the evaporating drop (S10) show the external resistance to be controlling over more than 70% of the evaporation process, when expressed in terms of the vapor to total mass ratio. However, if the time dependence of the evaporation process is considered, the very beginning of the evaporation process, where internal resistance is controlling, is found to take up some 50% of the total evaporation time. Thus some exchanger volume may be saved if the volatile liquid is introduced in saturated state, preferably with some initial vapor content. The approximate predominance of the individual film coefficients as function of the evaporation ratio and time is shown in Fig. 17, where the external resistance controlling factor is defined as U/h_c. The approximate individual and over-all heat-transfer coefficients, calculated per unit of effective liquid–liquid contact area, are shown in Fig. 18. Detailed studies of the initial evaporation stages of single drops are presently underway (P4).

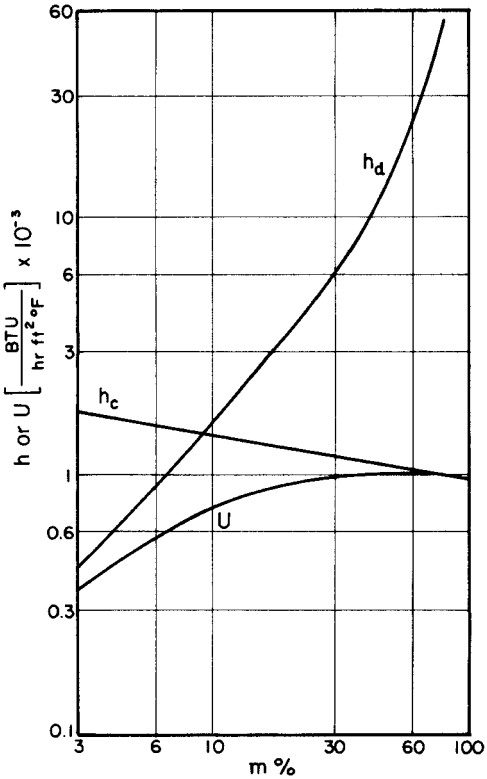

FIG. 18. Estimated individual and over-all heat-transfer coefficients—pentane drop (3.6 mm diam) evaporating in water (S10).

As the heat-transfer area varies during the evaporation process, the overall heat-transfer coefficient is best defined in relation to the initial drop area. By calculating the overall resistance to heat transfer directly from the temperature driving force, the total evaporation time and the total heat content of the drop, Sideman, Hirsch, and Gat (S11a) obtained a relationship between the average overall heat-transfer coefficient and the initial diameter. For single pentane drops evaporating in sea water,

$$\bar{U}^* = 1.05 \times 10^4 d^{*-0.64} \tag{48}$$

when $\bar{U}^*$ is expressed in Btu/hr/ft^2/°F and d^* is in millimeters. Direct plotting of the average experimental instantaneous heat-transfer coefficients (Fig. 19)

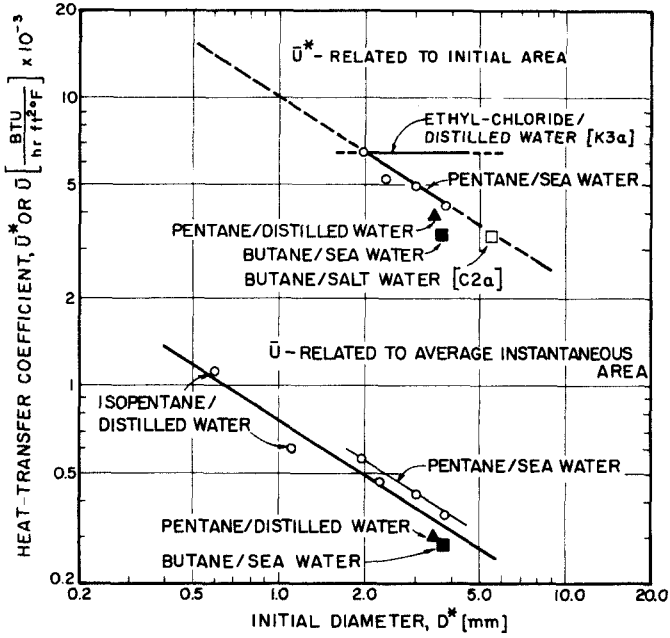

FIG. 19. Heat-transfer coefficients as a function of initial drop diameter (S11a).

for all the hydrocarbon-water systems tested (including condensation of isopentane in water), related to the total area of the rising two-phase drop, gives

$$\bar{U} = 0.76 \times 10^3 d^{*-0.64} \tag{49}$$

The constant for the pentane–sea-water system alone is 0.882×10^3.

The independence of $\bar{U}^*$ on the initial drop diameter exhibited by Klipstein's (K3a) data in Fig. 19 is most probably due to the nucleation technique employed by him whereby a sharp electric power pulse was given

to each drop through a nichrome heating wire in contact with the drop (S11a). In contrast, all the other data reported here, including those for butane in 24% NaCl-water solution (C2a), were obtained by allowing the bubbles to nucleate naturally in unaerated systems.

Comparison of the above equations shows that the characteristic average of the total instantaneous transfer area is some 12 times larger than the initial area, or some 35% of the final area of the completely evaporated drop. This is in accord with the smaller evaporation rates in the beginning of the evaporation process shown in Figs. 17 and 18.

As seen from Fig. 19, the heat-transfer coefficient related to the initial drop area is about one order of magnitude larger than the one related to the "time average" of the instantaneous total area. However, if heat transfer is assumed to take place only between the volatile liquid at the bottom of the two-phase bubble and the continuous phase, then the liquid–liquid transfer coefficient can be approximated (S10) to be about 2.5 the value of $\bar{U}$. The corresponding coefficients for nonevaporating drops are about 60 Btu/ft^2/hr/°F, which is at least one order of magnitude lower than that of the values realized with the evaporating drops.

Some degree of superheating is required before nucleation sets in in the drop, depending on drop size as well as the physical and chemical purity of the fluids. Similar phenomena have also been observed in countercurrent spray column studies (S9), where the temperature of the continuous phase can be lowered to the desired value only after some evaporation starts. As is to be expected, the time required for complete evaporation of the drop is inversely proportional to the temperature driving-force. A similar relationship exists for the length of the evaporation path of single drops. This, however, may not be directly extended to populations of drops, where the onset of nucleation is not simultaneous but rather depends on the dispersed phase flow rate, holdup, and degree of turbulence of the system.

As shown in Fig. 16, a droplet leaving the nozzle at the bottom evaporates and grows while rising in the column. Three operating zones were noticed in the spray column operating with a multiorifice plate: a free-rising zone at the bottom, a turbulent zone, and a foam zone at the top of the column. In the free-rising zone, equivalent to the "streamline" region noted in gas–liquid contacting columns at low gas flow rates and low holdups, the evaporating drops rise unhindered. As the superficial velocity increases with vapor generation, the growing drops lose their individual identity, and coalescence as well as turbulence is observed. This turbulent zone is analogous to the turbulent region noted in gas–liquid systems at superficial gas velocities above approximately 10 ft/min. Obviously, the interfacial area decreases with increased coalescence. The foam height, which varied with the operating conditions from 10 to 50 mm, was not considered (S9) to contribute much to the

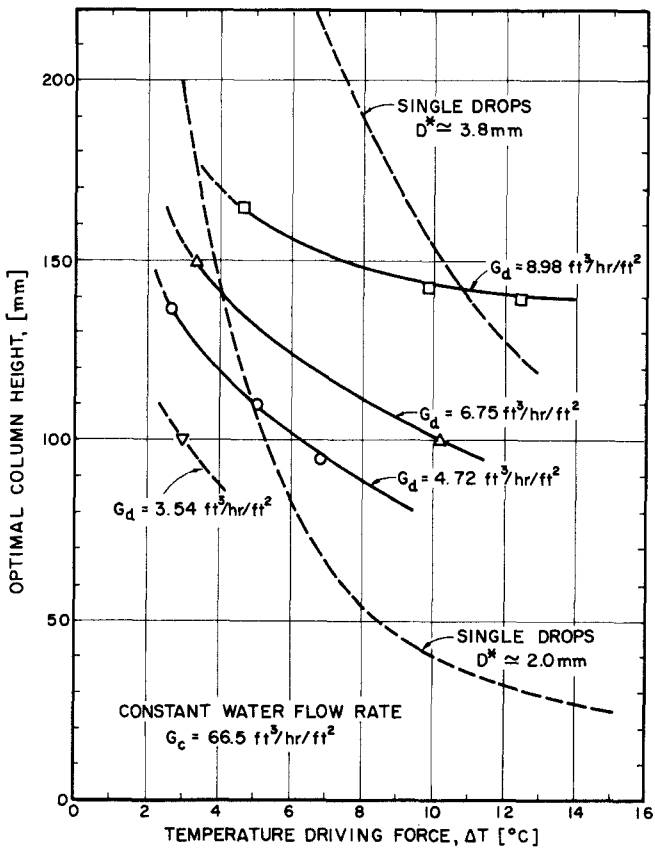

FIG. 20. Effect of temperature driving-force on optimal column height—pentane-water system (S9).

overall transfer area, but was included in the subsequent evaluation of the optimal column heights and the volumetric transfer coefficients.

In Fig. 20 the optimal column height (defined as the height in which evaporation is complete but no superheating of the vapors occurs) is plotted against the log-mean temperature driving-force at various dispersed-phase flow rates. It is noted that identical orifice velocities of pentane were used, and the initial diameter in all the runs shown was about 1.40 mm. Comparison with the single-drop data included in Fig. 20 allows some insight into the effect of drop interaction. Increasing the pentane flow rate at a constant temperature driving-force is equivalent to increasing the diameter of single drops. This is consistent with the observed increase in coalescence with increasing pentane flow rates. Also, the greater the coalescence, the smaller the effect of the temperature driving-force. Hence the effect of initial drop

diameter will decrease as the dispersed phase flow rate and the temperature driving-force are increased.

At a constant pentane flow rate (4.72 $ft^3/hr/ft^2$) the volumetric heat-transfer coefficient was found (S11a) to depend only slightly on the initial drop diameter. Approximately,

$$U_v \sim D^{*-0.1}$$

for $G_c = 66.5$ $ft^3/hr/ft^2$. The effect of the continuous-phase flow rate is generally small. An exponent of 0.135 was found for $G_c = 30.4$ $ft^3/hr/ft^2$. Evidently the effect of the initial drop diameter is mainly in the free-rise "streamline" zone in the lower part of the column. The upper "turbulent" zone is practically unaffected by the initial drop size, consistent with the independence of gas holdup and the specific interfacial transfer area relative to the orifice diameter at high gas flow rates that is observed in gas–liquid contacting systems.

The volumetric heat-transfer coefficients obtained in the countercurrent spray column are plotted against the mass flow-rate ratio in Fig. 21, allowing direct comparison with Fig. 14 where some of the analogous data for liquid–liquid spray columns are presented. For direct comparison with Table V, it is noted that the spray-column diameter was 2.75 in. with a total height of 33.5 in. Orifice diameter was 0.5 mm, and the number of orifices varied between 9 and 22 depending on the desired pentane flow rate. Holdup fraction varied from 0.12 to 0.22 at the range of flow rates indicated in Fig. 21, and the volumetric transfer coefficients varied from 4.8×10^3 to 12.1×10^3 $Btu/ft^3/hr°/F$. These results clearly demonstrate the higher efficiency of the three-phase exchanger as compared with the liquid–liquid heat exchangers.

For comparison with other evaporation studies, it is noteworthy that the data presented in Fig. 21 was obtained with a temperature approach of 1.7°C at the continuous-phase outlet, and that the pentane feed entered the nozzles subcooled by some 1.5°C. A reduction in the free-rising stream line zone is feasible with superheated dispersed-phase feeds and closer approach temperatures. This would greatly increase the volumetric transfer coefficient which is inversely proportional to the temperature driving-force and the optimal column height.

Harriott and Wiegandt (H10a) studied an upflow cocurrent flash evaporator in which pentane or methylene chloride was mixed with the water before entering the 2-in. column. A sieve plate with $\frac{1}{4}$- or $\frac{1}{8}$-in. holes was placed 1 ft upstream to facilitate dispersion. The volumetric transfer coefficients were estimated to be about 17×10^4 $Btu/hr/ft^3/°F$, based on an approach exit temperature of 0.5°C and a 1-ft length of pipe. This result is similar to that reported by Wilke *et al.* (W10) for a cocurrent pipe evaporator, and is about one order of magnitude larger than that reported for the countercurrent spray

column. As in the case of liquid–liquid exchangers, this is probably due to better atomization of the dispersed phase and the closer temperature approaches measured in the cocurrent pipe-type exchangers.

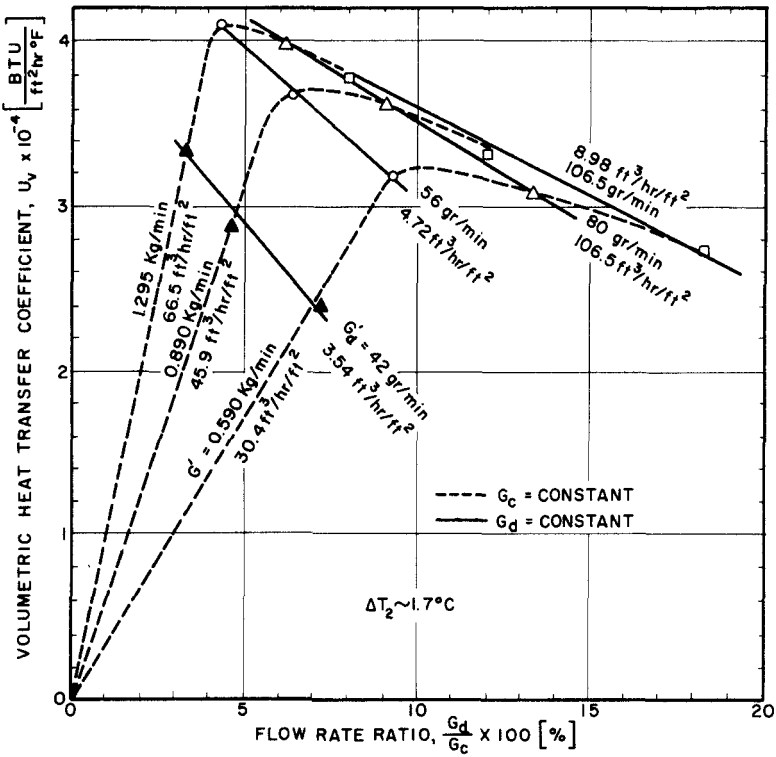

FIG. 21. Volumetric heat-transfer coefficient as a function of G_d/G_c; ΔT_2 = constant; pentane-water.

Mechanical agitation increases the rate of evaporation. This is due to increase of interfacial area with drop breakup, heterogeneous nucleation, and higher turbulence. By combining the concept of local isotropy in turbulent agitation together with the particular characteristics of the volatile drops evaporating in immiscible media, Sideman and Barsky (S8a) related the specific heat flow rate (per unit volume) to the specific power input P_v of the agitator and the temperature driving-force. Using small-scale as well as pilot-plant data, they demonstrated that the general form of the derived relationships

$$q_v \sim P_v^{\,x} \Delta T^y \tag{50}$$

holds even for nonhomogeneous mixtures as well as for evaporation at liquid–

liquid interfaces, where local isotropy may not exist. The exponents x and y vary with operating conditions, the controlling mixing regimes (viscous, kinetic, or coalescence preventing), and mixing intensity. The exponents decrease with increased coalescence and decrease of the mixing intensity, as is evident from Fig. 22. For completely dispersed systems at high mixing

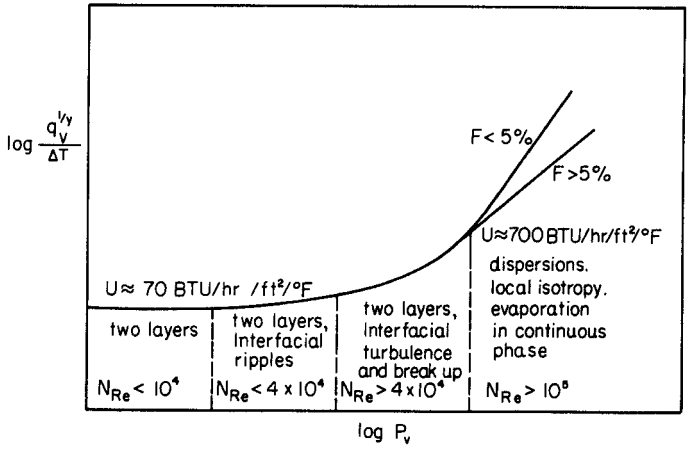

FIG. 22. A general presentation of the effect of specific power input and turbulence intensity on heat transfer between a nonvolatile liquid and an immiscible, volatile, evaporating liquid. $N_{Re} = Nd^2\rho_c/\mu_c$ (S8a).

intensity, $x = 8$–12 and $y = 4$–6, depending on the dispersed-phase holdup and the mixing regime. For the practical case of operating with some excess butane in sea water (H10a), where a butane layer floats above the continuously agitated fluid, $x = 3.84$ and $y = 1.54$. Values of $x = 0.08$ and $y = 1.43$ were found for heat transfer between agitated water and pentane layers at $(N_{Re})_{mixer}$ between 1 and 4×10^4. At lower mixer Reynolds numbers, $x = 0$. The contact area is well defined; q_A, the heat flow rate per unit area, may replace q_v, and Eq. (50) reduces to the well-known boiling correlation

$$q_A \sim \Delta T^y \tag{50a}$$

For the pentane–water system, $y = 1.42$, in good agreement with the exponent of 1.33 calculated for turbulent natural convection and commonly applied to surface boiling. For nucleate boiling of a single component, the value of the exponent in Eq. (50a) reported in the literature varies between approximately 2.5 and 5. Comparison with the exponents given above for the two-component three-phase system seems to indicate that, although the evaporation in the latter system is of the surface-evaporation type, the hydrodynamic

effects associated with high turbulence are responsible for the high heat-transfer coefficients realized in these systems.

Some elaboration on boiling heat transfer at liquid–liquid interfaces (without external mixing) is instructive. A comparison of all available interfacial boiling data is presented in Fig. 23. Note that the slope of the lines n is

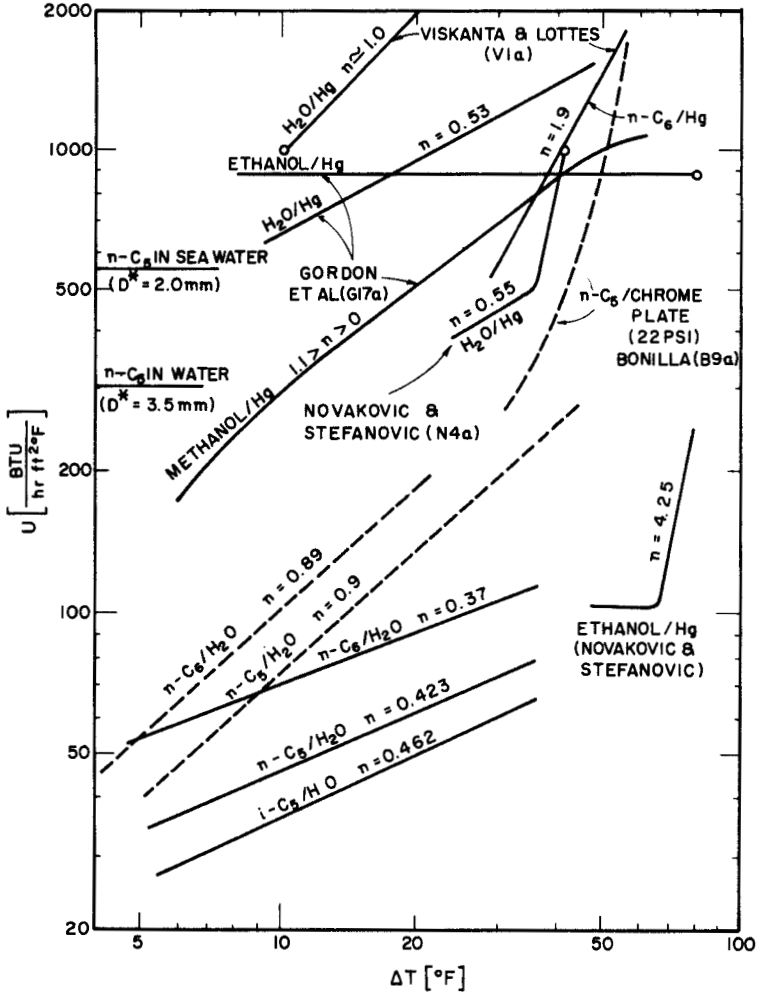

FIG. 23. Comparison of boiling data from liquid surfaces.

equal to $y - 1$ since, by definition, $U = q_A \Delta T$. The dotted lines for the n-pentane and n-hexane were obtained by seeding the water interface with artificial nuclei. The ensuing higher evaporation rates are seen by the larger

slopes of these lines as compared with those obtained with clean water interfaces. These results are consistent with Novakovic and Stefanovic's (N4a) observations on the effects of surface contamination and boiling from the walls of the vessel on the apparent transfer coefficients. The differences in the data of Novakovic, Gordon (G17a), and Viskanta (V1a) obtained in boiling from the mercury interface shown in Fig. 22 is thus readily explained: neither Gordon nor Viskanta used deaerated mercury; thus, "boiling usually started at lower superheats . . . because of the presence of contaminants and gases absorbed and adsorbed on the mercury surface" (V1a). Moreover, since thick mercury layers were used in these two studies, large oscillations and bouncing (G17a) of the mercury interface were evident at high heat fluxes. Whereas Novakovic's data, taken with thin mercury layers (3–6 mm) and with extreme precaution to avoid contamination and wall effects, indicate a transformation from surface to nucleate boiling, the data of Viskanta and Gordon (as well as ours with a seeded interface) represent some averages of these two basic boiling mechanisms.

Also included in Fig. 23 are Bonilla's data (B9a) for nucleate boiling of pentane from a chrome-plated heater, as well as the average over all heat-transfer coefficient, related to the instantaneous overall heat-transfer area, for pentane drops evaporating while rising in water. As noted earlier, the heat-transfer coefficient in the latter case was found to be practically independent of the temperature driving-force in the range studied (up to 15°C).

In conclusion, it is evident from Figs. 22 and 23 that the rate of heat-transfer increases with increasing interfacial turbulence, irrespective of whether this turbulence is induced by high heat fluxes (as in Gordon's mercury surface), induced boiling by artificial nucleation sites (gas or solid contaminants), or mechanical agitation at the liquid–liquid interface.

B. Condensation of Bubbles in Immiscible Liquid Media

The related work of Bankoff and Mason (B2) on latent heat transfer from steam bubbles condensing in a turbulent subcooled water stream casts light on this interesting phenomenon. A train of steam bubbles was injected into a submerged jet of subcooled water. Depending on the steam flow rate, water temperature, and velocity, three distinct types of bubble behavior could be distinguished: (*1*) ellipsoid bubbles with smooth surface at low steam rates and high temperature gradients (90–130°F); (*2*) ellipsoid bubbles with irregular surface at increased steam flow rates and about 90°F temperature gradient; and (*3*) irregular bubbles which (unlike the first two groups) did not completely collapse at the lower temperature gradients (30–50°F).* The surface heat-transfer coefficients for all three groups varied between 13,000 and

* The relative significance of the effects of the liquid inertia and the heat transfer on the collapse rate was recently reported (F1a).

316,000 Btu/hr/ft^2/°F, with Reynolds numbers varying from 172 to 14,000. The frequency of the bubbles varied between 200 to 2500 cps. Empirical equations for the Nusselt number as function of the Peclet and Strouhal numbers are given (B2) for the three different bubble groups.

The transfer coefficients reported by Bankoff compare favorably with those reported by Grassmann and Wyss (G19), who studied heat transfer between steam bubbles and water. With a bubble frequency of about 20/sec, they obtained water-side coefficients ranging from 14,000 to 20,000 Btu/hr/ft^2/°F. Superheated vapor-side coefficients were 40–160 Btu/hr/ft^2/°F. Bankoff's higher values are undoubtedly due to the highly turbulent nature of his system.

The analogous studies of direct-contact condensation involving immiscible fluids are rather meager. Sideman and Hirsch (S11) have recently reported some low-speed cinecamera studies of single isopentane bubbles condensing while rising in stagnant water. Two different nozzles of 3 and 6 mm i.d. were used in this work, resulting in initial bubble diameters of about 3.8 and 5.5 mm. The smaller bubbles usually appear as ellipsoids with relatively small fluctuations in shape. The larger bubbles deform appreciably, appearing in various shapes, such as disks, cones, saucers. A typical sequence of condensation of the larger size bubble is shown in Fig. 24. The greatest changes in the volume and area of the bubbles occur at the initial stages of the evaporation process. This so-called "turbulent" region of high deformation extends up to some 80–90 wt = % of liquid content in the bubble. In the second "laminar" region, the transfer rate decreases appreciably as the internal resistance to heat transfer gradually dominates the rate of heat transfer.

The characteristics of the instantaneous heat-transfer coefficients are basically similar (but in reverse) to those found earlier in the complementary study of evaporating drops, leading to the conclusion that here too most of the heat transfer takes place at the liquid–liquid interface. Absolute comparison based on liquid or vapor fraction in the two-phase particle is difficult, since some condensation takes place during bubble formation; despite prior superheating of the bubble, the exact amount of liquid in the initial bubble is unknown. Also, in the range of small temperature driving-forces studied (up to 6°F), condensation was not spontaneous and not complete. Unlike the evaporation studies (Fig. 16), no distinction between the vapor and the volatile liquid in the bubble could be observed at these low temperature-differences. Condensation was complete only at higher temperature driving-forces, allowing clear distinction of the phases in the condensing bubbles similar to that shown in Fig. 16 for the initial evaporation stages.

The suggested similarity of the heat-transfer mechanism in evaporation and condensation in immiscible media is substantiated by the similar characteristics of the data when plotted as instantaneous Nusselt vs Reynolds

numbers, and the good agreement of the condensation data with the values predicted by Eq. (47) (S11). The general agreement of the average over-all condensation heat-transfer coefficients with those of evaporation is also evident in Fig. 19.

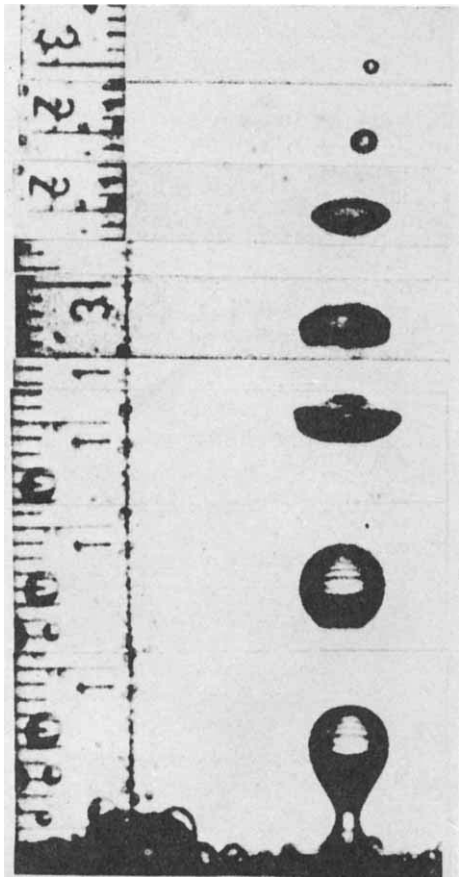

FIG. 24. Isopentane bubble condensing in water (S11).

It is interesting to note that the two phases in the bubble were distinct in the presence of air in the bubble. An analysis of the pictures of a condensing isopentane-air bubble indicated no effect of the presence of air on the condensation rate. However, more work is required before a final conclusion can be drawn, especially since all available information regarding condensation on solid surfaces as well as condensation of steam bubbles in water (G19)

indicates a decrease in the condensation rate in the presence of non-condensable gases. Similarly, the presence of an inert gas in CO_2 bubbles in water reduced the absorption mass-transfer coefficient by some 20 to 40 percent (L4). It is not yet clear whether this latter effect is due to smaller radial motion of the contracting bubble, to internal surface resistance, or to formation of an insulating gas cap on top of the bubble; should the latter be the cause, this would hardly affect the over-all transfer coefficient for condensation, which is apparently mostly controlled by the external resistance to transfer at the liquid–liquid interface.

In agreement with the single-drop evaporation studies, no significant effects of the temperature difference on the heat-transfer coefficient were observed in the narrow temperature range studied. An attempt to isolate these effects is presently underway, especially since the temperature driving-force was found to affect the initial and final liquid content of the bubble (S11) as well as the volumetric coefficient (W9).

The overall transfer coefficients (related to the overall transfer area) obtained in this three-phase two-component condensation study were about 600 and 1100 Btu/hr/ft^2/°F for the large and small bubbles, respectively. These compare favorably with the values reported for condensation of steam in water, which are, however, one order of magnitude larger. The difference is reasonable in view of the possibility for mass diffusion at the gas–liquid interface in the two-phase steam–water system, as well as the much higher turbulence encountered, especially in Bankoff's system (B2).

Wiegandt (W9) studied isobutane condensation in an ice-packed column, utilizing small temperature gradients. The experimental data reported indicate a decrease in the volumetric heat-transfer coefficients from 1000 to 660 Btu/hr°F/ft^2 (column cross section) with increasing temperature driving-force from 2 to 7°F. Although only small effects of the temperature gradient on the transfer coefficients in latent heat transport have been reported (S12, W9, W10), extrapolation of data of large ΔT to small temperature gradients (to about 1°C, which is of practical interest for economic reasons) may be erroneous, mainly since hydrostatic-head effects on the normal boiling temperature are very pronounced at small ΔT's.

Condensation studies of butane in water-ice slurries in a 2-in. diam column were also reported (W9), indicating increasing condensation rates with increasing ice content of the slurry. With a butane feed rate of 1.24 lb/ft^2/min and an average temperature gradient of 6°F, the overall heat transfer coefficient is reported to be 2000 Btu/hr/°F/ft^2 (column cross section).

Direct-contact condensation of steam in Aroclor, with a venturi as mixing device, was reported by Lackey (L1). Working with temperature gradients of about 10, 40, and 70°F between the two fluids, he observed a strong effect of the temperature gradients on the steam flow rate, the latter decreasing

strongly with decreasing temperature gradient. The apparent volumetric heat-transfer coefficients reported are in the range of 150,000–400,000 Btu/hr/ft^3/°F.

The heat-transfer characteristics of condensing steam in Aroclor in a simulated cocurrent spray column were also reported (L1). The volumetric heat-transfer coefficient, in Btu/hr/ft^3/°F, was assumed directly proportional to the steam flow rate W_d, and is given by

$$U_v = 9.2 \times 10^3 W_d \tag{51}$$

where W_d is measured in lb/hr.

Direct condensation of methylene chloride in a cocurrent downflow sieve-plate condenser in a 6-in. pipe was reported by Harriott and Wiegandt (H10a). Transfer coefficient, based on average condensation and exit liquid temperatures and the turbulent bubbling froth area only (0.09 ft^2), were from 70,000 to 100,000 Btu/hr/ft^2/°F, increasing with superficial gas velocity from about 1 to 2.2 ft/sec. The corresponding volumetric coefficients are up to 400,000 Btu/hr/ft^3/°F, based on 3-in. froth height.

For condensation of methylene chloride in water, in cocurrent downflow 4-in. and 6-in. diam columns packed with $\frac{1}{2}$-in. Intalox saddles, the volumetric transfer coefficients reported (H10a) were less than half those obtained with the sieve-plate column. The difference may be due partially to the different definition of the temperature driving-force applied for these two columns. (The log-mean ΔT was used for the packed bed, and a 2-in. transfer height was assumed.) The volumetric heat transfer coefficients "increased with the 0.4–0.6 power of the liquid rate" from 65,000 to 150,000 Btu/hr/ft^3/°F with the liquid rate increasing from 1 to 4×10^4 lb/hr/ft^2. Contrary to the sieve-plate and spray-column studies, no effects of the vapor flow rate (from 1100 to 2500 lb/hr/ft^2) on the heat-transfer coefficient were noted in the packed bed study.

Wilke *et al.* (W10) reported data on steam condensation in countercurrent flow with Aroclor in 2- and 3-feet-high 12-in. diam columns packed with 1-in. Raschig rings. The experimental HTU_L (liquid-resistance-controlling height of a transfer unit) varied from 0.8 to 1.5 ft for Aroclor flow rates of 1.5 to 3×10^4 lb/hr/ft^2, corresponding to over-all transfer coefficients of about 6000 Btu/hr/ft^3/°F (H10a). The comparison between these two studies is difficult, as different condensation heights were used in evaluating the transfer coefficients. Smaller area with the 1-in. rings, the higher viscosity of Aroclor, and possible channeling in countercurrent flow may explain some of the difference.

It is noteworthy that spray-column exchangers are usually more efficient than packed beds for systems yielding small drops and consequent higher transfer area per unit column volume. However, because of pressure drop

through the liquid and backmixing in the column, packed beds may be preferred.

Some attempts to predict the volumetric heat-transfer coefficients were also reported. Hu (H19) suggested a design procedure for packed towers for use as direct-contact gasoline condensers. Hu's technique was later severely criticized by Lackey (L1), who presented a detailed procedure for determining the *HTU* by analogy to, and based on data of (S7), liquid-film controlling mass transfer in gas–liquid systems (W10). [An equation for calculating the *HTU* for the gas desuperheating section is also given (W10.] A somewhat different procedure to predict the volumetric heat-transfer coefficients in packed beds was suggested by Harriott and Wiegandt (H10a), who applied the penetration theory for the heat- and mass-transfer analogy. Application of the mass-transfer analogy (oxygen desorption data) to condensation in sieve plates (H10a) seems unsatisfactory.

In concluding this chapter on heat transfer with change of phase it is noted that, despite the advantages and effectiveness realized in utilizing latent heat transport, relatively little is known on the basic mechanism of this important phenomenon, and the various factors affecting it. It is probably instructive to note that the high heat-transfer coefficients obtained due to turbulence at the surface of these rapidly growing or contracting two-phase particles are comparable to those realized in nucleate boiling.

VI. Miscellaneous Effects on Heat Transfer

A. Drop and Column End Effects

All equations and relationships reviewed in Sections III and IV and summarized in Tables I–III refer to the constant-velocity region of transfer. Drop end effects, associated with drop formation and coalescence, may sometimes affect the transfer to a considerable degree and should be taken into consideration. Numerous workers (G8, G12, G23, H13, L11, L13, S6, W6) have attempted to isolate the end effects. A relationship designed to distinguish between the overall and end transfer efficiencies was proposed by Johnson and Hamielec (J2).

The transfer efficiency in the drop-formation region varies approximately as the square root of the drop-formation time and inversely as the drop diameter. Since the drop acceleration interval is quite short, acceleration effects are normally combined with drop-formation effects. Heertjes (H13), basing his analysis on Higbie's penetration theory, suggested equations for the drop-formation and coalescence regions. For the drop-formation region,

$$E_{f1} = 10.3\left(\frac{\alpha\Theta}{\pi R^2}\right)^{0.5} \tag{52}$$

where Θ is the time of drop formation. Somewhat different relations were derived by Licht (L13) and by Groothuis and Kramers (G23) who applied different procedures to the same basic assumptions.

Assuming that coalescence time is equal to drop-formation time, and that the drop spreads at the interface of the two phases, exposing a fresh film of area $\bar{A}$, it can be shown (S8) that the ratio of transfer efficiencies in the drop-formation and coalescence regions can be approximated by

$$\frac{E_{f1}}{E_{f2}} \approx 1.75 \frac{A}{\bar{A}} \tag{53}$$

where A is the drop surface area. Assuming that a drop with a diameter of 1 mm spreads to 5–10 mm diam, the transfer efficiency in the coalescence region is 3–15 times that of the drop-formation region. This consideration applies only if the new drop forms a fresh surface at the contact area between the phases, which obviously is far from reality.

A simple relationship exists between the overall end-effect transfer efficiency E_F, the transfer efficiency in the constant velocity region E_m, and the over-all transfer efficiency E_T. Defining (1 − E) as the "complementary efficiency," it can be shown that

$$1 - E_F = \frac{1 - E_T}{1 - E_m} \tag{54}$$

Experimental data can be used to determine E_F. As expected, E_F depends on the drop diameter as well as on the nozzle design. Experiments (J2) with 2.8-mm-diam cyclohexanol drops, falling in water out of a flat nozzle at 25°C, gave a complementary end effect, $1 - E_F$, of 0.81; whereas for a 4.3-mm drop from a sharp-edged nozzle (45°), the complementary value was only 0.78.

In spite of occasional pronounced drop end effects, they are commonly neglected in practice. This is especially justified in industrial units, where drop formation is rapid and the constant-velocity region is quite large, usually due to overdesign of the column. However, column end effects, associated with the longitudinal-dispersion and flow patterns in spray columns, strongly affect the transfer efficiency of the column.

Column end effects, though on a larger scale, are sometimes considered analogous to those associated with drop formation. The latter undoubtedly contributes to increase the former. However, no quantitative relationships between drop and column end effects are as yet known for countercurrent operation. As suggested by Vermeulen and others, the concentration (or temperature) of each incoming stream increases or decreases abruptly on entering the column. In contrast, the concentration pattern for each outgoing stream becomes flat as it approaches its outlet, and no discontinuity is

observed at this end (M6). As mentioned in connection with Pierce's spray-column studies (P3), the sharp drop in the driving force is especially pronounced in the continuous-phase inlet region, and was found to be almost independent of continuous-phase inlet nozzle and column design (G14). These phenomena are attributed to recirculation ("backmixing") of the continuous phase (P3), longitudinal dispersion (M6) or continuous phase envelopes (G15a) or wakes (L5a) carried with the dispersed phase.

Complete temperature profiles in the column, rather than external end values, are required for proper evaluation of the true transfer coefficients, the longitudinal-dispersion coefficient, and the column end effects. Geankoplis (G15) measured concentration profiles inside the column to determine the "true" transfer coefficients, and suggested a procedure for correlating tower and effects in terms of a fictitious height of column. Miyauchi and Vermeulen (M6) have provided a general theoretical treatment, which permits evaluation of the over-all behavior of two-phase countercurrent flow by considering the effect of longitudinal dispersion of both fluids. A trial-and-error procedure was suggested for determining inlet discontinuity as a measure of column performance on the basis of interior concentration data at the inlet and outlet ends. "Jump ratios" are available to facilitate trial-and-error calculation of the individual Peclet numbers from experimental data. (Peclet numbers here are defined in terms of the effective longitudinal-dispersion coefficient of each phase.) A method for calculating the maximum transfer efficiency by approximate determination of the "number of over-all dispersion units" is also presented (M6). The analytical solutions and graphs presented should allow for quantitative treatment of the data.

In a recent study of mixing in spray-column heat exchangers, Letan and Kehat (L5a) have shown that the temperature jump occurs only at the inlet of the continuous phase, i.e., water. This sharp discontinuity, a measure of the amount of mixing in the column, was found to be a function of the holdup fraction of the dispersed phase (kerosene) and the ratio of flow rates of the two phases. A hydrodynamic model based on the idea that considerable transfer to and from the drop occurs on the downstream side of the drops, to a terroidal vortex downstream of the drops, successfully explains the temperature profiles obtained by Letan and Kehat, as well as in other extraction studies. A high portion of the heat is transferred from the drops to the wakes at the bottom of the column, and a high portion of this heat is transferred to the continuous phase by the wakes shed in the middle of the column. This model can explain the flat temperature profiles at the bottom of the column, and the rise of the temperature of the continuous phase in the middle of the column. New material from the upstream side of the drop enters the circulating core of the wake through the boundary layer and is shed at a higher temperature some time later higher in the column. At the upper section of the

column the drop temperature becomes constant, and the rate of heat transfer diminishes to zero. At the top of the column, the holdup of the drops increases rapidly, and the detached wakes mix with the inlet water stream which immediately loses its original identity, similar to a liquid entering a highly mixed system. At the same holdup fraction, the total amount of water carried in the wakes up the column increases with increasing the flow ratio, resulting with greater mixing and higher jump ratios. At $F = 0.24$, the jump ratio rose from 0.1 to 0.55 when the flow rate ratio increased from 1 to 3.5.

At low holdups, longitudinal dispersion due to continuous-phase velocity profiles controls the amount of mixing in the countercurrent spray column; whereas at higher holdups the velocity profile flattens, and the shed-wake mechanism controls. Above holdups of 0.24, the temperature jump ratio is linearly proportional to the dispersed-to-continuous-phase flow ratio, and all mixing is caused by shed wakes into the bulk water and coalescence of drops. As column size decreases, it approaches the characteristics of a perfect mixer, and the jump ratio approaches unity (as compared with the value of zero for true countercurrent flow). It is interesting to note that changing the inlet temperature of dispersed phase by about 55°F hardly affected the jump ratio, probably due to the balancing effects of reduced viscosities and a decrease of drop diameter.

B. Temperature and Temperature-Gradient Effects

Temperature obviously affects the physical properties of the fluids, thus indirectly affecting the transfer coefficients. As in the case of heat transfer in pipes, equations involving viscosity corrections for temperature differences between bulk and interface have been suggested (Eq. II-14, Table II) and are especially applicable for viscous continuous phases. No correction is needed for water, for instance, especially at $(N_{Re})_c > 50$. At lower $(N_{Re})_c$, natural convection is pronounced, especially in liquid systems with low kinematic viscosity. Since the transfer coefficient for natural convection is a function of the Grashof number, one may expect some effects of the temperature gradient. Steinberger and Treybal's equation (Eq. 6) allows for these effects.

As already mentioned, the viscosity of the dispersed phase affects the maximum obtainable transfer coefficients in spray-column operation; lower viscosities allow higher coefficients at lower operating temperature level. For the "hot-top" spray column, a linear dependence of the transfer coefficients and the fluidity of the dispersed phase was found (T2). This phenomenon may also be associated with reduction in surface tension. A decrease in drop diameter and increase in transfer area per unit volume of column may then be expected to increase the volumetric transfer coefficients.

The temperature gradient in heat exchangers is commonly expressed in

terms of the apparent log-mean temperature, which is computed from end temperatures of incoming and outgoing streams and is based on the assumption of a linear temperature gradient between top and bottom. This is evidently not the actual situation in countercurrent spray columns, due to backmixing and end effects associated with irregular flow patterns. True temperature profiles are required to obtain the true driving-force. Different inlet and outlet conditions correspond to the same externally apparent column performance, whereas a unique situation exists inside the column for any specific set of conditions. The difference and the relation of the transfer coefficients, derived from true, apparent (external ends), and measured interior temperature profiles in the column is demonstrated by Miyauchi and Vermeulen (M6) in their theoretical study of longitudinal dispersion in countercurrent two-phase operations.

The log-mean average is highly sensitive to the approach temperature at the columns ends, requiring highly accurate measurements of the true temperatures. Thus, the lower the approach temperature, the higher becomes the uncertainty of the calculated results. In these cases, recourse to the arithmetic-mean average should probably be advisable, to ensure more "conservative" design data. For a 1° approach temperature at one end and a 5° temperature difference at the other end, the ratio of the logarithmic- and arithmetic-mean temperature gradients is 1.25. For a given constant flow ratio of one of the fluid streams, the mean temperature is a function of the flow rate as well as of the absolute temperatures of the other streams. Li (L10) observed that a certain relationship exists between the apparent log-mean temperature, and the volumetric transfer coefficient. By manipulating the temperature at the ends of the column, Gardner (G1) obtained, for the specific case of $G_c = 20$ ft/hr and $(G_d/G_c) = 1$,

$$U_v = 2000(\Delta T)_{\ln}^{-0.146} \tag{55}$$

Contrary to suggestion (G1), Eq. 55 cannot be used for other flow conditions, because $(\Delta T)_{\ln}$ is in itself a function of the flow-rate ratio.

Consider a special case of a spray column, where the temperature of one phase, say the dispersed phase, is constant throughout. This situation is ideally obtained when the dispersed phase is volatile and evaporates while rising in the column. Under ideal operating conditions (no subcooling or superheating), with constant mass flow rate of the dispersed phase,

$$(GC_p\rho\ \Delta T)_c = \text{const}, \qquad \text{or} \qquad \Delta T_c \propto 1/G_c \tag{56}$$

and the mean temperature gradient will vary accordingly. This case is similar, though not identical, to the special case of negligible concentration change

in one phase treated by Miyauchi and Vermeulen (M6), where

$$M = (GC_p\rho)_c/(GC_p\rho)_d = \Delta T_d/\Delta T_c$$

In that case, $M \to 0$ since $\Delta T_d \to 0$ and Colburn's equation (M6, Eq. 11), derived for piston flow (apparent external transfer coefficient), reduces to

$$U_v = \frac{q}{V(\Delta T)_{\ln}} = \frac{(GC_p\rho)_c}{Z} \ln \frac{T_{c2} - T_d}{T_{c1} - T_d} \tag{57}$$

The latter is obviously obtained independently (and for all M) from the definition of the over-all volumetric transfer coefficient, based on apparent exterior temperatures. The obvious and common technique of studying column performance is to keep G_d and T_{c1} (in) constant and vary G_c until the desired minimum approach temperature is obtained, corresponding to $(G_c)_{\min}$, Fig. 25(a). Now, since T_{c2} (out) ideally approaches T_d only asymptotic-

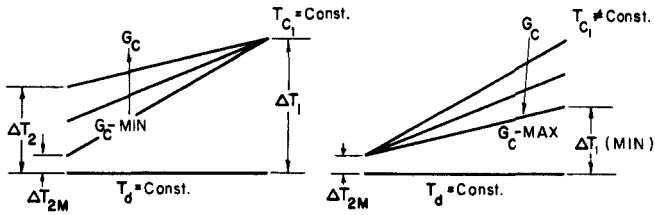

FIG. 25. Schematic presentation of column operation: (a) constant continuous-phase inlet temperature; (b) constant continuous-phase outlet temperature.

ally, a minimum practical approach-temperature gradient, ΔT_{2M}, is set in practice. Obviously, for any $G_c > (G_c)_{\min}$, we get $\Delta T_2 > \Delta T_{2M}$. Since $(\Delta T)_{\ln} > [(\Delta T)_{\ln}]_{\min}$, hence, $U_v < (U_v)_{\text{"min"}}$. This is demonstrated in Fig. 26, curve A, for the system pentane–water (S9), which shows that for a given dispersed-phase mass flow rate and a constant T_{c1} the transfer coefficient decreases with increasing continuous-phase flow rate. Similar, almost parallel, curves are obtained for different continuous-phase inlet temperature. As shown by curve B of Fig. 26, the opposite conclusion is also true, if the column is operated under the restrictions of constant ΔT_{2M}. Under these conditions [Fig. 25(b)] G_c can theoretically increase to infinity, thus decreasing ΔT_1 and $(\Delta T)_{\ln}$. Practical limitations, such as flooding, holdup, etc., would however dictate $(G_c)_{\max}$. Thus, at any $G_c < (G_c)_{\max}$, we obtain $\Delta T_1 > (\Delta T_1)_{\min}$, hence, $(\Delta T)_{\ln} > [(\Delta T)_{\ln}]_{\min}$ and $U_v < (U_v)_{\max}$. Thus, curve B of Fig. 26 is the locus of all points of optimum operating conditions, yielding $(G_c)_{\min}$ and $(U_v)_{\text{"min"}}$ for any desired T_{c1}. Similar curves are obtained for other values of ΔT_{2M}, as well as for different values of G_d, permitting determination of the optimum

operating conditions. The advantage of working at minimum approach temperature is obvious. The above analysis may be extended to include longitudinal effects, along the lines suggested in (M6). Similar reasoning may

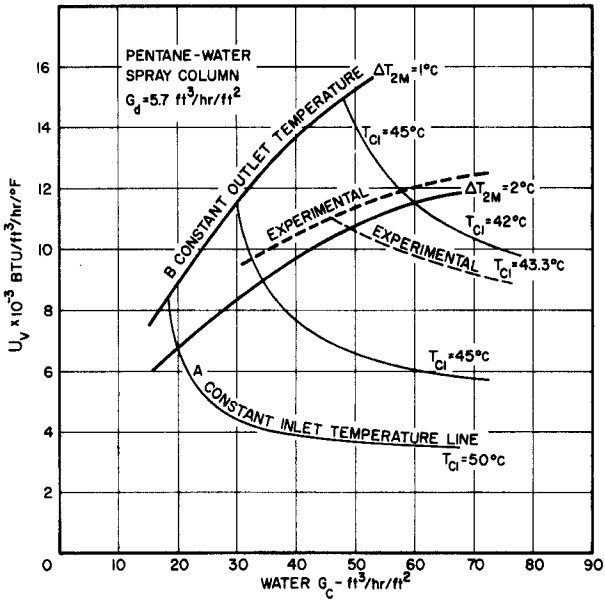

FIG. 26. Effect of inlet and outlet temperatures on volumetric heat-transfer coefficients in three-phase spray-column heat exchanger—pentane–water system.

probably apply to other two-phase two-component systems, where $M \neq 0$. No attempt has been made to extend the analysis beyond this point.

C. Effect of Drop Diameter on Heat-Transfer Coefficient

Within the drop-size range of practical interest, there seems to be general agreement that drops may be classified in two main size categories, "small" (below 1–3 mm diam) and "large" (2–7 mm diam). As will be discussed later, the exact transition value depends on the physical properties of the system involved. "Small" drops are similar in behavior to solid particles, whereas "large" drops exhibit higher transfer coefficients. In the transition zone between the "small" and "large" categories, transfer coefficients change abruptly, as shown by Calderbank and Moo-Young (C2) and Thorsen and Terjesen (T3). This change in the transfer coefficients can be attributed to the onset of circulation in the transition zone. In the absence of circulation, the external Nusselt number varies as the $\frac{1}{3}$ power of the Prandtl number, while

in its presence the Prandtl exponent may be $\frac{1}{2}$. Garner *et al.* showed that internal circulation sets in at a Reynolds number of about 20. Terjesen *et al.* (T3) attributed the large increase in heat-transfer coefficient to an increase in velocity and vortex formation behind the drop above a Reynolds number of about 25. Since the higher transfer rates are certainly associated with the mobility of the drops' interface, we can leave aside the question as to whether circulation induces heat transfer directly or indirectly due to higher drop velocity and larger angle of separation. Experimental evidence of both schools indicates that transition from "small" to "large" drop behavior is governed by the Reynolds number, hence by velocity and fluid viscosity.

Calderbank and Moo-Young (C2) suggested two different correlations for the two drop-size ranges, substantiating it with an impressive amount of heat- and mass-transfer experimental data of various workers. Their equation for "small" drops or bubbles is

$$(N_{\mathrm{Nu}})_c = 2 + 0.31(N_{\mathrm{Ra}})^{1/3} \tag{58}$$

and for drops and bubbles larger than 2–3 mm,

$$(N_{\mathrm{Nu}})_c = 0.42\left(\frac{\Delta\rho g D^3 \rho_c}{\mu_c^2}\right)^{1/3} (N_{\mathrm{Pr}})_c^{1/3} \tag{59}$$

Equations (58) and (59) indicate the transfer coefficient to be independent of the drop diameter. This conclusion, however, should be accepted with caution.

Beginning with the small drops, assumed to behave like solid spheres, the transfer coefficient can be plotted against drop diameter according to the classical Froessling equation or Eq. (5) originally derived for a solid sphere. Such a plot (H10) shows an almost straight line for diameters of 0.1–2.3 mm, as might have been expected. (In this size range the terminal drop velocity is approximately proportional to the diameter.) Below 50–200 μ, however, the transfer coefficient should increase with decreasing diameter, since the Nusselt number can never fall below 2, its limit for diffusion in a stagnant medium.

Experimental work with drops and bubbles of 2–7 mm diam indicates rather small changes in heat-transfer coefficient with changing drop diameter. Experiments (B1, B11, G26, H4, L13) with aqueous solutions showed very small decrease in the transfer coefficient with increasing diameter, as may be expected from Eq. (18). Only absorption experiments (H4) in glycol solutions showed a large increase in the transfer coefficient in the same size range. This, however, may be accounted for by the low Reynolds numbers involved.

Relatively little experimental evidence not favoring the practical independence of the transfer coefficients from drop diameter within the above size

ranges is available. Hammerton and Garner's (H4) experimental work on water absorption of CO_2 and ethylene bubbles (2–3 mm diam) showed that the transfer coefficients, as well as bubble velocity, are directly proportional to the bubble diameter. Spence and Streeton (S19) reported similar relationship for extraction of uranyl nitrate from organic solvent (butex) to water drops, ranging in diameter from 0.5 to 5 mm. However, this relationship is heavily biased by a few values for the smallest and largest drops.

An hypothesis assigning Garner's results to a transition zone was recently refuted by new evidence. Leonard and Houghton (L4) substantiated Hammerton and Garner's observations in their work on water absorption of CO_2 bubbles, 2–5 mm diam. The close relationship between bubble diameter and bubble velocity, as well as between bubble diameter and transfer coefficient, indicates that hydrodynamic relationships exist between the bubble velocity and the transfer coefficient. The higher velocities of immiscible bubbles (such as nitrogen and helium in water), compared with miscible (CO_2) bubbles, raises questions as to the possible effect of transfer rates on bubble velocity (D3). Some dependence of rate of transfer and concentration on drop velocity is also indicated by Spence's data (S19); it is of interest to note that experiments have shown (L4) that immiscible bubble velocity decreases with increasing diameter up to 6 mm, whereas that of miscible bubbles increases in the same range.

Baird and Davidson (B1) derived an equation for the transfer coefficient of very large bubbles. Based on Davies and Taylor's model of potential flow past a spherical cap (D7), this relationship predicts a decrease in transfer with increasing bubble diameter, as does Eq. (18). For large bubbles or high Reynolds numbers, the transfer coefficient varies as the $-\frac{1}{4}$th power of the diameter. The experimental data with bubbles up to 20 mm diam are of the order of magnitude predicated by these equations, although a slight *increase* of the transfer coefficient with increasing diameter is observed. Bubbles larger than 25 mm exhibited unstable transfer rates (B1, L4). A detailed comparison between experimental gas absorption data and theoretical relationship between the transfer coefficient and the equivalent spherical diameter (up to 3 cm) is given by Calderbank and Lochiel (C1a).

As already stated, the high transfer coefficients exhibited by "large" drops and bubbles (above 2–3 mm diam) is closely related to the presence or absence of circulation. Therefore any outside factors affecting drop circulation, such as impurities and surface-active agents, will naturally affect the relationship between drop size and transfer coefficient. This is especially true in the transitional drop-size range of 1–3 mm, where the presence of surface-active agents affects the transfer coefficient by a factor of two to three, depending on whether the drop falls into the "small" or "large" category.

A workable criterion for the transitional drop radius is given (L8) by

$$R_{cr} \approx \left[\frac{3}{g}\frac{\sigma - \sigma_s}{\rho_d - \rho_c}\right]^{1/2} \tag{60}$$

which is based on the maximum decrease in the interfacial tension σ of a pure system to σ_s observed in solutions of the given surface-active agents.

Experimental evidence (B13, T3) shows the effect of surface-active agents on transfer coefficients of noncirculating drops to be negligible, while quite significant in "large" drops near the transition zone. In the presence of surface-active agents, velocities of drops up to 4 mm diam were found (T3) almost identical with those of solid particles of the same diameter, and the coefficients were accordingly small. However, pure drops gave much higher coefficients with little dependence on drop diameter within the same size range. It may be concluded that the presence of surface-active impurities affects the behavior of a drop as "small" or "large," but has almost no effect in either "small" or "large" drops once the classification is made. Surface-active agents affect the boundary flow conditions by inducing viscous stresses. Hence the effect of surface-active agents decreases at higher ratios of the inertial to viscous forces, i.e., higher Reynolds numbers. For a given system, the larger the drops (or bubbles) and the higher their velocity, the smaller the effect of surface-active agents (B1, L8). Bubbles in the range of 4.5 to 10 mm indicated no effect of the presence of surface-active agents (L8), and neither did larger bubbles of up to 40 mm diam (B1).

The relationships between drop diameter, internal and external resistance to transfer, and overall transfer rates in agitated liquid–liquid systems are shown by Nagata and Yamaguchi (N1). As also found in solid–liquid agitated systems, the smaller the difference in density between the two phases, the smaller is the effect of increasing agitator speed (and decreasing drop diameter) on reducing the continuous-phase resistance. The drop-side transfer efficiency decreases with increased agitation. Large drops ($\approx$1.0 mm diam) at the lower agitation range (100–200 rpm) indicated high transfer efficiencies, comparable to the mixed-drop model. The transfer efficiency of small drops (0.1–0.05 mm) associated with higher agitation speeds ($\approx$1000 rpm) approached the theoretical molecular-diffusion values. However, as the values of the over-all transfer rate calculated by the mixed-drop and rigid-drop theories approach each other for small drops at high agitation speeds, the effect of agitation on the internal transfer efficiency becomes insignificant. In general, the effect of increasing agitation intensity is mainly to increase the interfacial transfer area, hence the volumetric transfer coefficient. An almost linear relationship between these is indicated. The obvious advantages of the higher residence

time, associated with agitated systems, on the transfer process is irrelevant to the problem at hand.

Coalescence, hence drop size, is sometimes strongly promoted by the transfer of solute from droplets to the ambient continuous phase. The recent experimental work of Groothuis and Zuiderweg (G24) showed that the addition of about 1.5 wt = % of solute to the dispersed phase increased the average drop size by up to 80%, while increasing coalescence rates about twenty-fold, which is equivalent to the effect of a forty-fold increase in power input. Larger drops were found at higher holdup ratios, which is consistent with the data obtained in these laboratories (Fig. 13) in spray-column heat-transfer studies.

In spray columns smaller drops have a lower terminal as well as slip velocity at the same holdup, and flooding points appear at lower (G_d/G_c) ratios and lower holdups. As shown by Elgin's (W4) correlation, at a given slip velocity holdup decreases with decreasing drop diameter. However, the transfer area per unit column volume increases inversely with drop diameter and the transfer coefficient should increase accordingly. This, as well as the interrelationships between drop diameter, holdup, and slip velocity, explains the independence of spray-column performance, over a fairly wide range, of the nozzle diameter.

VII. Related Works

A number of works closely related to the subject of heat transfer to a single drop were not incorporated in this chapter but should be borne in mind when dealing with this problem. These are works dealing with the mechanism of drop formation (B5, D4, H6, H11, H12, H21, N4, N6), the hydrodynamics of drops and bubbles, their drag and velocities (E3, G17, G18, H3, H7, K3, L7, M1, M4, N5, R3a, R4, S2, S5, W7, Z1, Z2), and interfacial agitation (D5, S21). In addition, certain important factors affecting transfer rates were not included or elucidated. Among these are oscillation (C6, G12, H9, H20, H21, L9, L12, S15), vortex formation behind a moving drop (G2, G10, G12, L6), natural convection (G4, G20, S20, T7), turbulence (C2, H5, H8, L8, N2), surface tension (G5, H1, H16, L8, L15, L17, S4, S15, W5), and interfacial resistance (S4) and drop frequencies (B11).

Acknowledgments

The author acknowledges with thanks the financial support of the Israel National Council for Research and Development, which enabled this work to be carried out. Thanks are due to Mr. E. Goldberg of the Technion, Israel Institute of Technology, for editorial advice.

Nomenclature

A Surface area of drops
$\bar{A}$ Surface area of spread drop in coalescence zone, Eq. (53)
A_n Constants
a Constant, Eqs. (4)
B Ratio of heat capacities of disperse to continuous phase, Eq. (32)
b Constant, Eq. (4)
C_n Constant, Eqs. (32), (33), (47)
C_p Specific heat capacity
D Drop diameter
D^* Initial drop diameter
$\bar{D}$ Column diameter
d Agitator diameter, Fig. 22
E Reciprocal of Biot number, Eqs. (32), (33)
E_{f_1} Transfer efficiency, drop-formation region
E_{f_2} Transfer efficiency, coalescence region
E_F Transfer efficiency, end effects, over-all $(=E_{f_1} + E_{f_2} - E_{f_1}E_{f_2})$
E_m Transfer efficiency, constant-velocity region
E_T Transfer efficiency, over-all
F Holdup, fractional volume of dispersed phase in column
f Coefficient, function of $(N_{Re})_c$
G Superficial velocity, $ft^3/hr/ft^2$
G' Mass velocity, $lb/hr/ft^2$
g Acceleration; coefficient, viscosity-dependent
H Rate of heat transfer, $Btu/hr/ft^2$
h Heat-transfer coefficient, $Btu/hr/ft^2/°F$
K Log-mean average of distribution coefficients, Eq. (2)
K_v Ratio of true to potential-theory interfacial velocity
k Thermal conductivity, $Btu/hr/ft/°F$
L Geometric factor $(D + \bar{D}/\bar{D})$, Eq. (2)
M $(GC_p\rho)_c/(GC_p\rho)_d = 1/B$
m Exponent, Eq. (4); per cent vapor in two-phase drop
N Rate of agitator, rpm, Fig. 22
n Exponent, Eq. (4); also $y - 1$, Fig. 23
P_v Specific power input
Q Total heat transferred, Btu, Eq. (12)
q heat flow, Btu/hr, Eq. (31)
q_A Heat-transfer rate, $Btu/hr/ft^2$
q_V Specific heat flow rate, $Btu/hr/ft^3$
$\bar{R}$ Factor, ratio of effective to molecular diffusivity
R Drop radius
r Radial distance
S Reciprocal of Peclet number, Eqs. (32), (33)
T Temperature
ΔT Temperature difference between phases
U Overall heat-transfer coefficient, $Btu/hr/ft^2/°F$
$\bar{U}$ Overall transfer coefficient, related to average of instantaneous area
$\bar{U}^*$ Overall transfer coefficient, related to initial drop area
U_v Volumetric over-all heat transfer coefficient, $Btu/hr/ft^3/°F$
u Drop velocity, relative
u_s Velocity at drop equator, Eq. (16)
V Volume, of drop or column
V_s Slip velocity, Eq. (39)
W Mass-flow rate (lb/hr)
x Distance vector, parallel to drop interface, Eq. (15); exponent, Eq. (50)
y Distance vector, normal to drop interface, Eq. (15); exponent, Eq. (50)
Z Height of column

Greek letters

α Molecular diffusivity, ft^2/hr
α_e Eddy diffusivity, ft^2/hr
β Coefficient of thermal expansion; opening half angle of vapor in evaporating drop
η External resistance controlling factor, U/h_c
σ Surface tension
σ_s Surface tension at high concentration of surface-active agent
Θ Time
λ Eigenvalue
μ Viscosity

ν Kinematic viscosity
ρ Density
ϕ Angle, Eq. (16)
ψ Stream function, Eq. (16)
ω Radius, dimensionless, Eq. (25)

DIMENSIONLESS GROUPS

N_{Bi} Biot number, $[h_c R/k_d]$
N_{Fo} Fourier number, $[=\alpha\Theta/D^2]$
N_{Gr} Grashof number, $[=D^3 g\rho_c \Delta\rho/\mu_c{}^2]$ or $[D^3 g\beta \Delta T/\nu^2]$
K Log-mean average of partition coefficients, Eq. (2)
L Geometric factor, $[=(D+\bar{D})/\bar{D}]$, Eq. (2)
N_{Nu} Nusselt number, $[=hD/k]$
N_{Pe} Peclet number, $[=Du/\alpha]$
N_{Pe}' Peclet number, modified, Eq. (26)
N_{Pr} Prandtl number, $[=\mu C_p/k]$
N_{Ra} Rayleigh number, $[=D^3 g\,\Delta\rho/\mu_c\alpha_c]$
N_{Re} Reynolds number, $[=Du\rho/\mu]$
N_{We} Weber number, $[=\rho u^2 D/\sigma]$

SUBSCRIPTS

1 Inlet, continuous phase
2 Outlet, continuous phase
$2M$ Outlet, minimum approach temperature
c Continuous phase
co Continuous phase, outlet
cr Critical, radius, Eq. (60)
cz Continuous phase, at height z
d Dispersed phase, drop
i Inlet
0 Outlet
s Surface-active agent, slip (velocity)
t Total
v Volumetric, overall

TABLE AI

VALUES FOR EQ. (11) (E2)

$\frac{h_c D}{k_d}$	λ_1	λ_2	λ_3	λ_4	A_1	A_2	A_3	A_4
4	2.029	4.913	7.979	11.086	0.159	0.00634	—	—
6	2.289	5.087	8.096	11.173	0.153	0.0109	—	—
8	2.456	5.233	8.205	11.256	—	—	—	—
10	2.570	5.354	8.303	11.335	0.142	0.0179	0.00408	—
12	2.654	5.454	8.391	11.409	—	—	—	—
14	2.717	5.538	8.470	11.477	0.134	0.0220	0.00600	—
16	2.765	5.608	8.541	11.541	—	—	—	—
18	2.804	5.667	8.603	11.599	0.129	0.0242	0.0119	0.00291
20	2.836	5.717	8.659	11.653	—	—	—	—
22	2.863	5.761	8.708	11.703	0.125	0.0255	0.00858	0.00359
32	2.948	—	—	—	0.118	—	—	—
42	2.993	—	—	—	—	—	—	—
62	3.041	—	—	—	0.111	—	—	—
82	3.080	—	—	—	—	—	—	—
102	3.080	—	—	—	0.107	—	—	—
00	—	—	—	—	—	—	—	—

TABLE AII

VALUES FOR EQ. (IV-4) ($h_c = \infty$)

n	λ_n	A_n	Reference
1	1.656	1.29	(E2)
2	9.08	0.596	
3	22.2	0.386	
4	38.5	0.35	(H13)
5	63.0	0.28	
6	89.8	0.22	
7	123.8	0.16	

TABLE AIII

VALUES FOR EQ. (IV-5) (E2)

$\frac{h_c D}{k_d}$	λ_1	λ_2	λ_3	A_1	A_2	A_3
3.20	0.262	4.24	—	1.49	0.107	—
5.33	0.386	—	—	—	—	—
8.00	0.534	—	—	—	—	—
10.7	0.680	4.92	—	1.49	0.300	—
16.0	0.860	5.26	—	1.48	0.382	—
21.3	0.982	5.63	—	1.47	0.428	—
26.7	1.082	5.90	15.7	1.49	0.495	0.205
53.3	1.324	7.04	17.5	1.43	0.603	0.298
107	1.484	7.88	19.5	1.39	0.603	0.384
213	1.560	8.50	20.8	1.31	0.588	0.396
320	1.600	8.62	21.3	1.31	0.583	0.391
00	1.656	9.08	22.2	1.29	0.596	0.386

REFERENCES

A1. Akselrud, G. A., *Zh. Fiz. Khim.* **28**, 1446 (1953).

B1. Baird, M. H. I., and Davidson, J. F., *Chem. Eng. Sci.* **17**, 87 (1962).

B1a. Baird, M. H. I., and Hamielec, A. E., *Can. J. Chem. Eng.* **40**, 119 (1962).

B2. Bankoff, S. G., and Mason, J. P., *A.I.Ch.E.* (*Am. Inst. Chem. Engrs.*) *J.* **8**, 30 (1962).

B3. Barbouteau, I., *Rev. Inst. Franc. Pétrole Ann. Combust. Liquides* **11**, 358 (1956).

B4. Bartok, W., and Mason, S. G., *J. Colloid Sci.* **13**, 293 (1958).; **14**, 13 (1959).

B5. Baston, J. B., M.S. thesis, Univ. Tennessee, Knoxville, Tennessee, 1951.

B6. Bentwich, M., Szwarcbaum, B., and Sideman, S., *8th Natl. Heat Transfer Conf., Los Angeles, Calif.*, 1965, ASME Paper 65-HT-38 (1965).

B7. Beyaert, B. O., Lapidus, L., and Elgin, J. C., *A.I.Ch.E.* (*Am. Inst. Chem. Engrs.*) *J.* **7**, 46 (1961).
B8. Bond, W. N., *Phil. Mag.* [7] **57**, 890 (1927).
B9. Bond, W. N., and Newton, D. R., *Phil. Mag.* [7] **57**, 794 (1928).
B9a. Bonilla, C. F., and Cichelle, M. T., *Trans. Am. Inst. Chem. Engrs.* **41**, 755 (1945).
B10. Boussinesq, M., *J. Math. Pures Appl.* **1**, 285 (1905); *Ann. Chim. e Phys.* (*Paris*) **29**, 364 (1913).
B11. Bowman, C. W., and Johnson, A. I., *Can. J. Chem. Eng.* **40**, 139 (1962).
B12. Bowman, C. W., Ward, D. M., Johnson, A. I., and Trass, O., *Can. J. Chem. Eng.* **39**, 9 (1961).
B13. Boye-Christensen, G., and Terjesen, S. G., *Chem. Eng. Sci.* **9**, 225 (1959).
B14. Brenner, H., *Chem. Eng. Sci.* **18**, 109 (1963).
B15. Brown, G., *ASME, Proc. Gen. Discussion Heat Transfer* 1951, p. 41.
B16. Brown, W. S., Pitts, C. C., and Leppert, G., *Am. Soc. Mech. Engrs., Paper* **61-SA-26** (1961).
C1. Calderbank, P. H., and Korchinski, I. J. O., *Chem. Eng. Sci.* **6**, 65 (1956).
C1a. Calderbank, P. H., and Lochiel, A. C., *Chem. Eng. Sci.* **19**, 485 (1964).
C2. Calderbank, P. H., and Moo-Young, M. B., *Chem. Eng. Sci.* **16**, 39 (1961).
C2a. Canning, F. T., personal communication (1965).
C3. Carr, B. B., *Chem. Eng. Progr.* **59**, 59 (1963).
C4. Carslaw, H. S., and Jaeger, J. C., "Conduction of Heat in Solids," 2nd ed., p. 235, Oxford Univ. Press, London and New York, 1959.
C4a. Chao, B. F., *Phys. Fluids* **5**, 69 (1962).
C5. Conkie, W. R., and Savic, P., *Natl. Res. Council Can. Rept.* **MT-23** (1953).
C6. Constan, G. L., and Calvert, S., *A.I.Ch.E.* (*Am. Inst. Chem. Engrs.*) *J.* **9**, 109 (1963).
C7. Coulson, J. M., and Skinner, S. J., *Chem. Eng. Sci.* **1**, 197 (1952).
D1. Danckwerts, P. V., *Trans. Faraday Soc.* **47**, 1014 (1951).
D2. Danckwerts, P. V., *Ind. Eng. Chem.* **43**, 1460 (1951).
D3. Datta, R. L., Napier, D. H., and Newitt, D. M., *Trans. Inst. Chem. Engrs.* (*London*) **28**, 14 (1950).
D4. Davidson, J. F., and Schuler, B. O. G., *Trans. Inst. Chem. Engrs.* (*London*) **38**, 335 (1960).
D5. Davies, J. T., and Rideal, E. K., "Interfacial Phenomena," Academic Press, New York, 1961.
D6. Davies, J. T., *56th Ann. Meeting, A.I.Ch.E., Houston, Tex.*, Dec. 1963.
D7. Davies, R. M., and Taylor, G. I., *Proc. Roy. Soc.* **A200**, 375 (1950).
D8. Deindoerfer, F. H., and Humphrey, A. E., *Ind. Eng. Chem.* **53**, 755 (1961).
E1. Eckenfelder, W. W., and Barnhart, E. L., *42nd Natl. Meeting A.I.Ch.E., Atlanta*, (1960).
E2. Elzinga, E. R., and Banchero, J. T., *Chem. Eng. Progr., Symp. Ser.* **55**, 149 (1959).
E3. Elzinga, E. R., and Banchero, J. T., *A.I.Ch.E.* (*Am. Inst. Chem. Engrs.*) *J.* **7**, 394 (1961).
F1. Fleming, J. F., and Johnson, H. F., *Chem. Eng. Progr.* **49**, 497 (1953).
F1a. Florschuetz, I. W., and Chao, B. F., *ASME J. Heat Transfer* **82**, 209 (1965).
F2. Friedlander, S. K., *A.I.Ch.E.* (*Am. Inst. Chem. Engrs.*) *J.* **3**, 43 (1957).
F3. Frisch, H. L., *J. Chem. Phys.* **22**, 123 (1954).
F4. Frossling, N., *Beitr. Geophys.* **52**, 170 (1938).
F5. Frumkin, A., and Levich, V. G., *Zh. Fiz. Khim.* **21**, 1183 (1947).
G1. Gardner, R. P., *At. Energy. Comm. Contract* AT-(40-1)-1320 (1958); M.S. Thesis in Chem. Eng., North Carolina State College, Raleigh, North Carolina, 1958.
G2. Garner, F. H., *Trans. Inst. Chem. Engrs.* (*London*) **28**, 88 (1950).

G3. Garner, F. H., Foord, A., and Tayeban, M., *J. Appl. Chem.* **9**, 315 (1959).
G4. Garner, F. H., and Grafton, R. W. *Proc. Roy. Soc.* **A224**, 64 (1954).
G5. Garner, F. H., and Hale, A. R., *Chem. Eng. Sci.* **2**, 157 (1953).
G6. Garner, F. H., and Hayock, P. J., *Proc. Roy. Soc.* **A252**, 457 (1957).
G7. Garner, F. H., and Lane, J. J., *Trans. Inst. Chem. Engrs.* (*London*) **37**, 162 (1959).
G8. Garner, F. H., and Skelland, A. H. P., *Trans. Inst. Chem. Engrs.* (*London*) **29**, 315 (1951).
G9. Garner, F. H., and Skelland, A. H. P., *Ind. Eng. Chem.* **46**, 1255 (1954).
G10. Garner, F. H., and Skelland, A. H. P., *Chem. Eng. Sci.* **4**, 149 (1955).
G11. Garner, F. H., and Suckling, R. D., *A.I.Ch.E.* (*Am. Inst. Chem. Engrs.*) *J.* **4**, 114 (1958).
G12. Garner, F. H., and Tayeban, M., *Anales Real Soc. Espan. Fis. Quim.* (*Madrid*) (**B56**), 479 and 491 (1960).
G13. Garwin, L., and Smith, B. D., *Chem. Eng. Progr.* **49**, 591 (1953).
G14. Geankoplis, C. J., and Hixon, A. N., *Ind. Eng. Chem.* **42**, 1142 (1950).
G15. Geankoplis, C. J., Wells, P. L., and Hawk, E. L., *Ind. Eng. Chem.* **43**, 1843 (1951).
G15a. Geankoplis, C. J., *Ind. Eng. Chem.* **44**, 2458 (1952).
G16. Geddes, A. P., *Trans. Am. Inst. Chem. Engrs.* **42**, 79 (1946).
G17. Gibbons, J. H., Houghton, G., and Coull, J., *A.I.Ch.E.* (*Am. Inst. Chem. Engrs.*) *J.* **8**, 274 (1962).
G17a. Gordon, K. F., Singh, T., and Weissman, E. Y., *Intern. J. Heat Mass Transfer* **3**, 90 (1961).
G18. Grassmann, P., and Reinhardt, A., *Chem.-Ing.-Tech.* **33**, 348 (1961).
G19. Grassmann, P., and Wyss, E., *Chem.-Ing.-Tech.* **34**, 755 (1963).
G20. Griffith, R. M., Ph.D. thesis, Univ. Wisconsin, Madison, Wisconsin, 1958.
G21. Griffith, R. M., *Chem. Eng. Sci.* **12**, 198 (1960).
G22. Grober, H., *Z. Ver. Deut. Ing.* **69**, 705 (1925).
G23. Groothuis, H., and Kramers, H., *Chem. Eng. Sci.* **4**, 17 (1955).
G24. Groothuis, H., and Zuiderweg, F. J., *Chem. Eng. Sci.* **19**, 63 (1964).
G25. Grover, S. S., and Knudsen, J. G., *Chem. Progr., Symp. Ser.* **51**, 71 (1955).
G26. Guyer, A., and Pfister, X., *Helv. Chim. Acta* **29**, 1173 and 1400 (1946).
H1. Haberman, W. L., and Morton, R. K., David Taylor Model Basin Rept. No. 802. U.S. Navy Dept., Washington, D.C., 1953.
H2. Hadamard, J., *Compt. Rend.* **152**, 1735 (1911).
H3. Hamielec, A. E., and Johnson, A. I., *Can. J. Chem. Eng.* **40**, 41 (1962).
H4. Hammerton, D., and Garner, F. H., *Trans. Inst. Chem. Engrs.* (*London*) **32**, S18 (1954).
H5. Handlos, A. E., and Baron, T., *A.I.Ch.E.* (*Am. Inst. Chem. Engrs.*) *J.* **3** 127 (1957).
H5a. Hanson, C., and Ingham, J., *Brit. Chem. Eng.* **10**, 391 (1965).
H6. Harkins, W. D., and Brown, F. E., *J. Am. Chem. Soc.* **38**, 246 (1916); **41**, 499 (1919).
H7. Harmathy, T. Z., *A.I.Ch.E.* (*Am. Inst. Chem. Engrs.*) *J.* **6**, 281 (1960).
H8. Harriott, P., *Can. J. Chem. Eng.* **40**, 60 (1962).
H9. Harriott, P., *Chem. Eng. Sci.* **17**, 149 (1962).
H10. Harriott, P., *A.I.Ch.E.* (*Am. Inst. Chem. Engrs.*) *J.* **8**, 93 (1962).
H10a. Harriott, P., and Wiegandt, H. F., *A.I.Ch.E.* (*Am. Inst. Chem. Engrs.*) *J.* **10**, 755 (1964).
H11. Hayes, W., Hardy, B. W., and Holland, C. D., *A.I.Ch.E.* (*Am. Inst. Chem. Engrs.*) *J.* **5**, 318 (1959).
H12. Hayworth, C. B., and Treybal, R. E., *Ind. Eng. Chem.* **42**, 1174 (1950).
H13. Heertjes, P. M., Holve, W. A., and Talsma, H., *Chem. Eng. Sci.* **3**, 122 (1954).

H14. Henniker, J. C., *Rev. Mod. Phys.* **21**, 322 (1949).
H15. Higbie, R., *Trans. Am. Inst. Chem. Engrs.* **31**, 365 (1935).
H16. Holm, P., and Terjesen, S. G., *Chem. Eng. Sci.* **3**, 265 (1954).
H17. Hsu, N. T., and Sage, B. H., *A.I.Ch.E. (Am. Inst. Chem. Engrs.) J.* **3**, 405 (1957).
H18. Hsu, N. T., Sato, K., and Sage, B. H., *Ind. Eng. Chem.* **46**, 870 (1954).
H19. Hu, S., *Refining Engr.* **C-12**, 722 (1956).
H20. Hu, S., and Kinter, R. C., *A.I.Ch.E. (Am. Inst. Chem. Engrs.) J.* **1**, 42 (1955).
H21. Hughes, G. R. R., and Gilliland, E. R., *Chem. Eng. Progr.* **48**, 497 (1952).
J1. Jakob, M., "Heat Transfer," Vol. 1. Wiley, New York, 1949.
J2. Johnson, A. I., and Hamielec, A. E., *A.I.Ch.E. (Am. Inst. Chem. Engrs.) J*, **6**, 145 (1960).
J3. Johnson, A. I., Minard, G. W., Huang, C. J., Hansuld, J. H., and McNamara, V. M., *A.I.Ch.E. (Am. Inst. Chem. Engrs.) J.* **3**, 101 (1957).
J4. Johnstone, H. F., Pigford, R. L., and Chapin, J. H., *Trans. Am. Inst. Chem. Engrs*, **37**, 95 (1941).
K1. Karnofsky, G., and Steinhoff, P. F., *U.S. Office Saline Water, Saline Water Res. Develop. Progr. Rept.* **40** 1960.
K2. Kinzer, G. D., and Gunn, R., *J. Meteorol.* **8**, 71 (1951).
K3. Klee, A. J., and Treybal, R. E., *A.I.Ch.E. (Am. Inst. Chem. Engrs.) J.* **2** 444 (1956).
K3a. Klipstein, D. H., D.Sci. thesis, Mass. Inst. Technol., Cambridge, Massachusetts, 1963.
K4. Kramers, H., *Physica* **12**, 61 (1946).
K5. Kronig, R., and Brink, J. C., *Appl. Sci. Res.* **A2**, 142 (1950).
K6. Kronig, R., and Bruijsten, J., *Appl. Sci. Res.* **A2**, 439 (1950).
K7. Kusik, C. L., and Happel, J., *Ind. Eng. Chem., Fundamentals* **1**, 163 (1962).
L1. Lackey, D. L., UCRL-10339, M.S. thesis, Univ. California, Berkeley, California, 1961.
L2. Lamb, H., "Hydrodynamics," 6th ed., p. 200. Cambridge Univ. Press, London and New York, 1932.
L3. Langmuir, I., *Phys. Rev.* **12**, 368 (1918).
L4. Leonard, J. H., and Houghton, G., *Chem. Eng. Sci.* **18**, 133 (1963).
L5. Letan, R., and Kehat, E., *Rept. Israel Natl. Council Res. Develop., 1963* (in Hebrew).
L5a. Letan, R., and Kehat, E., *A.I.Ch.E. (Am. Inst. Chem. Engrs.) J.* **11**, 804 (1965).
L6. Levich, V. G., *Zh. Obshch. Khim.* **19**, 18 (1949).
L7. Levich, V. G., *Intern. Chem. Eng.* **2**, 78 (1962).
L8. Levich, V. G., "Physiochemical Hydrodynamics," Prentice-Hall, Englewood Cliffs, New Jersey, International Series, 1962.
L9. Lewis, J. B., and Pratt, H. R. C., *Nature* **171**, 1155 (1953).
L10. Li, S. C., M.S. Thesis, North Carolina State College, Raleigh, North Carolina, 1957.
L11. Licht, W., and Conway, C. J. B., *Ind. Eng. Chem.* **42**, 1151 (1950).
L12. Licht, W., and Narasimhamurty, G. S. R., *A.I.Ch.E. (Am. Ints. Chem. Engrs.) J.* **1**, 366 (1955).
L13. Licht, W., and Pansing, W. F., *Ind. Eng. Chem.* **45**, 1885 (1953).
L14. Lileeva, A. K., and Smirnov, N., *J. Appl. Chem. USSR (English Transl.)* **34**, 1103 and 1295 (1961).
L15. Lindland, K. P., and Terjesen, S. C., *Chem. Eng. Sci.* **5**, 1 (1956).
L16. Linton, W. H., Jr., and Sherwood, T. K., *Chem. Eng. Progr.* **46**, 258 (1950).
L17. Linton, M., and Sutherland, K. L., *Proc. 2nd Intern. Conf. Surface Activity*, Vol. 1, p. 494 (1957).

L18. Lochiel, A. C., and Calderbank, P. H., *Chem. Eng. Sci.* **19**, 471 (1964).
M1. Ma, S. T., *IBM J. Res. Develop.* **6**, 472 (1962).
M1a. Marsh, B. D., and Heideger, W. J., *Ind. Eng. Chem., Fundamentals* **4**, 129 (1965).
M2. McAdams, W. H., "Heat Transmission," 3rd ed. Mc-Graw Hill, New York, 1954.
M3. McDowell, R. V., and Myers, J. E., *A.I.Ch.E. (Am. Inst. Chem. Engrs.) J.* **2**, 384 (1956).
M4. Meksyn, D., *J. Aerospace Sci.* **25**, 631 and 664 (1958).
M5. Minard, G. W., and Johnson, A. I., *Chem. Eng. Progr.* **48**, 62 (1952).
M6. Miyauchi, T., and Vermeulen T., *Ind. Eng. Chem. Fundamentals* **2**, 113 (1963).
N1. Nagata, S., and Yamaguchi, I., *Mem. Fac. Eng. Kyoto Univ.* **22**, 249 (1960).
N2. Naisel, D. S., and Sherwood, T. K., *Chem. Eng. Progr.* **46**, 131 and 172 (1950).
N3. Newman, A. B., *Trans. Am. Inst. Chem. Engrs.* **27**, 310 (1931).
N4. Nordberg, S., *Dechema Monograph* **41** (1962).
N4a. Novakovic, M., and Stefanovic, M., *Intern. J. Heat Mass Transfer* **7**, 801 (1964).
N5. Novoselov, V. S., *A.R.S. J. (Suppl.) 31*, 686 (1961).
N6. Null, H. R., and Johnson, H. F., *A.I.Ch.E. (Am. Inst. Chem. Engrs.) J.* **4**, 273 (1958).
O1. Othmer, D. F., Benenati, R. F., and Goulandris, G. C., *Chem. Eng. Progr.* **59**, 63 (1963).
P1. Pasternak, I. S., and Gauvin, W. H., *Can. J. Chem. Eng.* **38**, 35 (1960).
P2. Pattle, R. E., *Trans. Inst. Chem. Engrs. (London)* **28**, 32 (1950).
P3. Pierce, R. D., Dwyer, O. E., and Martin, J. J., *A.I.Ch.E. (Am. Inst. Chem. Engrs.) J.* **5**, 257 (1959).
P4. Pinder, K. L., Univ. British Columbia, personal communication 1965.
P5. Porter, J. W., Ph. D. Thesis, Univ. of California, Berkeley, 1965.
P6. Porter, J. W., Goren, S. L., and Wilke, C. R. (to be published).
Q1. Quigley, C. J., Johnson, A. I., and Harris, B. L., *Chem. Eng. Progr., Symp. Ser.* **51**, 31 (1955).
R1. Radusch, R., *Chem.-Ing.-Tech.* **28**, 275 (1956).
R2. Ranz, W. E., *Chem. Eng. Progr.* **48**, 247 (1952).
R3. Ranz, W. E., and Marshall, W. R., Jr., *Chem. Eng. Progr.* **48**, 141 (1952).
R3a. Redfield, J. A., and Houghton, G., *Chem. Eng. Sci.* **20**, 131 (1965).
R4. Rosenberg, B., David Taylor Model Basin Rept. No. 727 (1950).
R5. Rosenthal, H., M.S. Thesis, New York University (1949).
R6. Ruby, G. L., and Elgin, J. C., *Chem. Eng. Progr., Symp. Ser.* **51**, 17 (1955).
R7. Ruckenstein, E., *Chem. Eng. Sci.* **10**, 22 (1959).
R8. Rumscheidt, D., and Mason, S. G., *J. Colloid Sci.* **16**, 210 (1961).
R9. Rybozynski, W., *Bull. Intern. Acad. Polon. Sci.* **A40** (1911).
S0. Sagar, D. V., Ramanujam, T. K., Krishnamurty, V. V. G., and Rao, C. V., *Indian J. Tech.* **3**, 79 (1965).
S1. Sakiadis, B. C., and Johnson, A. J., *Ind. Eng. Chem.* **46**, 1229 (1954).
S2. Satapathy, R., and Smith, W., *J. Fluid Mech.* **10**, 561 (1961).
S3. Savic, P., *Natl. Res. Council Can. Rept.* **MT-22** (1953).
S4. Schechter, R. S., and Farley, R. W., *Brit. Chem. Eng.* **18**, 1 (1963).
S5. Schlichting, H., "Boundary Layer Theory," p. 403. Pergamon Press. Oxford, 1955.
S6. Sherwood, T. K., Evans, J. E., and Longcor, J. V. A., *Ind. Eng. Chem.* **31**, 1146 (1939).
S7. Sherwood, T. K., and Holloway, C., *Trans. Am. Inst. Chem. Engrs.* **36**, 39 (1940).
S8. Sideman, S., and Shabtai, H., *Can. J. Chem. Eng.* **42**, 107 and 238 (1964).
S8a. Sideman, S., and Barsky, Z., *A.I.Ch.E. (Am. Inst. Chem. Engrs.) J.* **11**, 539 (1965).

S9. Sideman, S., and Gat, Y., *57th Natl. Meeting A.I.Ch.E., Minneapolis, 1965 A.I.Ch.E.* (*Am. Inst. Chem. Engrs.*) *J.* **12**, No. 2 (1966).
S10. Sideman, S., and Hirsch, G., *Israel J. Technol.* **2**, 234 (1964).
S11. Sideman, S., and Hirsch, G., *A.I.Ch.E.* (*Am. Inst. Chem. Engrs.*) *J.* **11**, 1019 (1965).
S11a. Sideman, S., Hirsch, G., and Gat, Y., *A.I.Ch.E.* (*Am. Inst. Chem. Engrs.*) *J.* **11**, 1081 (1965).
S12. Sideman, S., and Taitel, Y., *Intern. J. Heat Mass Transfer* **7**, 1273 (1964).
S13. Siemes, W., and Franke, M., *Chem.-Ing.-Tech.* **30**, 165 (1958).
S14. Skelland, A. H. P., and Cornish, A. R. H., *A.I.Ch.E.* (*Am. Inst. Chem. Engrs.*) *J.* **9**, 73 (1963).
S15. Skelland, A. H. P., and Welleck, R. M., *A.I.Ch.E.* (*Am. Inst. Chem. Engrs.*) *J.* **10**, 491 (1964).
S16. Sleicher, C. A., Jr., *A.I.Ch.E.* (*Am. Inst. Chem. Engrs.*) *J.* **5**, 145 (1959).
S17. Smith, G. C., and Beckman, R. B., *A.I.Ch.E.* (*Am. Inst. Chem. Engrs.*) *J.* **4**, 180 (1958).
S18. Spelles, K. E., *Proc. Phys. Soc.* (*London*) **B65**, 541 (1952).
S19. Spence, R., and Streeton, R. J. W., *Chem.-Process. Eng.* **44**, 597 (1963).
S20. Steinberger, R. L., and Treybal, R. E., *A.I.Ch.E.* (*Am. Inst. Chem. Engrs.*) *J.* **6**, 227 (1963).
S21. Sternling, C. V., and Scriven, L. E., *A.I.Ch.E.* (*Am. Inst. Chem. Engrs.*) *J.* **5**, 514 (1959).
T1. Tang, Y. S., Duncan, J. M., and Schweyer, H. E., *Natl. Advisory Comm. Aeron., Tech. Note* **2867** (1953).
T2. Thompson, W. S., Woodward, T., Shrode, W. A., Baird, E. D., and Oliver, D. A., *U.S. Office Saline Water, Saline Water Res. Develop. Progr. Rept.* **63** (1962).
T3. Thorsen, G., and Terjesen, S. G., *Chem. Eng. Sci.* **17**, 137 (1962).
T4. Timson, W. J., and Dunn, C. G., *Ind. Eng. Chem.* **52**, 799 (1960).
T5. Toor, H. L., and Marchello, J. M., *A.I.Ch.E.* (*Am. Inst. Chem. Engrs.*) *J.* **4**, 97 (1958).
T6. Treybal, R. E., "Liquid Extration," 1st ed, p. 328. McGraw-Hill, New York, 1951.
T7. Tsubouchi, T., and Sato, S., *Chem. Eng. Progr. Symp. Ser.* **56**, 285 (1960).
U1. Umano, S., *Japan. Govt. Chem. Ind. Res. Inst.* **54**, 9 (1959) (in Japanese).
U2. Umano, S., *Japan. Govt. Chem. Ind. Res. Inst.* **61**, 5 (1959) (in Japanese).
V1. Vermeulen, T., *Ind. Eng. Chem.* **45**, 1664 (1953).
V1a. Viskanta, R., and Lottes, P. A., *Proc. Heat Transfer Fluid Mech. Inst.* p. 171, 1962,
V2. Vliet, G. C., and Lepper, G., *Heat Transfer Conf., Buffalo., Buffalo, N.Y.*, ASME publication 60-HT-5 (1960).
W1. Wakeshima, H., and Takata, K., *J. Phys. Soc. Japan* **13**, 1398 (1958).
W2. Wakeshima, H., and Takata, K., Superheat of Droplets in mercury. Private communication (1962).
W3. Ward, D. M., Trass, O., and Johnson, A. I., *Can. J. Chem. Eng.* **40**, 164 (1962).
W4. Weaver, R. E. C., Lapidus, L., and Elgin, J. C., *A.I.Ch.E.* (*Am. Inst. Chem. Engrs.*) *J.* 5, 533 (1959).
W4a. Welleck, R. M., and Skelland, A. H. F., *A.I.Ch.E.* (*Am. Inst. Chem. Engrs.*) *J.* **11**, 557 (1965).
W5. West, F. B., Herman, A. J., and Chong, A. T., *Ind. Eng. Chem.* **44**, 625 (1952).
W6. West, F. B., Robinson, P. A., Morgenthales, A. C., Beck, T. R., and McGregor, D. K., *Ind. Eng. Chem.* **43**, 234 (1951).
W7. White, E. T., and Beardmore, R. H., *Chem. Eng. Sci.* **17**, 351 (1962).
W8. Wiegandt, H. F., *Natl. Acad. Sci.* Publication 568, 377 (1958).

W9. Wiegandt, H. F., *U.S. Office Saline Water, Saline Water Res. Develop. Progr. Rept.* **41** (1960).
W10. Wilke, C. R., Cheng, C. T., Ledesma, V. L., and Porter, J. W., *Chem. Eng. Progr.* **59**, 69 (1963).
W11. Williams, G. C., Sc.D. thesis in Chem. Eng., Mass. Inst. Techl., Cambridge, Massachusetts, 1942.
W12. Woodward, T., *Chem. Eng. Progr.* **57**, 52 (1961).
Y1. Young, N. O., Goldstein, J. S., and Block, M. J., *J. Fluid Mech.* **6**, 350 (1959).
Z1. Zwick, S. A., *J. Math. Phys.* **37**, 246 (1958).
Z2. Zwick, S. A., and Plesset, M. S., *J. Math. Phys.* **23**, 308 (1955).